Water Resources and Industry 31 (2024) 100230

Contents lists available at ScienceDirect

Water Resources and Industry

journal homepage: www.elsevier.com/locate/wri

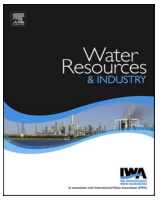

MXene-based composites for capacitive deionization – The advantages, progress, and their role in desalination - A review

Bakhtiar Ali Samejo [a,d], Kainat Naseer [b], Suraya Samejo [a], Farooque Ahmed Janjhi [c,d,***], Najma Memon [a,**], Roberto Castro-Muñoz [d,e], Grzegorz Boczkaj [d,f,*]

[a] National Centre of Excellence in Analytical Chemistry, University of Sindh, Jamshoro, Pakistan
[b] Faculty of Pharmacy, University of Karachi, Sindh, Pakistan
[c] Gdansk University of Technology, Faculty of Chemistry, Department of Process Engineering and Chemical Technology, 80 – 233, Gdansk, G. Narutowicza St. 11/12, Poland
[d] Gdansk University of Technology, Faculty of Civil and Environmental Engineering, Department of Sanitary Engineering, 80 – 233, Gdansk, G. Narutowicza St. 11/12, Poland
[e] Tecnologico de Monterrey, Campus Toluca, Av, Eduardo Monroy Cárdenas 2000, San Antonio Buenavista, 50110, Toluca de Lerdo, Mexico
[f] Adv. Mater. Center, Gdansk University of Technology, 80 – 233, Gdansk, G. Narutowicza St. 11/12, Poland

ARTICLE INFO

Keywords:
MXene
CDI
Electrode
Electrosorption
2D materials
Ion-selective separation

ABSTRACT

MXenes, a novel large family of 2D transition metal carbides, carbonitrides and nitrides are currently a "hot topic" in science due to their several fascinating physical and chemical properties. It follows from a rich diversity of their elemental compositions and chemical functionalities. MXenes can form composites with many substances, including polymers or metal oxides, which allows to effective "tune" MXene characteristics to a fit-to-the-purpose applications. Capacitive deionization (CDI) is currently widely studied as advanced desalination technique due to the advantages of cost-effectiveness, eco-friendly, and high salt removal capacity. One of key fields for CDI development relates to the ion's intercalation materials as concept taken from the sodium ion batteries, which is used in CDI because of their excellent desalination capacity. These materials provide effective sodium ions removal from the brine based on intercalation mechanism as well as redox reactions. In this review, we timely review an up-to-date accomplishment in the advancement of distinct MXene-based composite materials used as CDI electrodes, along with discussion of fundamental electrochemical energy storage mechanisms. The most relevant outcomes are highlighted together with the phenomena observed when applied in desalination applications. Finally, potential solutions as well as challenges in this field are summarized.

* Corresponding author. Gdansk University of Technology, Faculty of Civil and Environmental Engineering, Department of Sanitary Engineering, 80 – 233, Gdansk, G. Narutowicza St. 11/12, Poland.
** Corresponding author. National Centre of Excellence in Analytical Chemistry, University of Sindh, Jamshoro, Pakistan.
*** Corresponding author. Gdansk University of Technology, Faculty of Civil and Environmental Engineering, Department of Sanitary Engineering, 80 – 233 Gdansk, G. Narutowicza St. 11/12, Poland.
E-mail addresses: farooque.janjhi@pg.edu.pl (F.A. Janjhi), najma.memon@usindh.edu.pk (N. Memon), grzegorz.boczkaj@gmail.com, grzegorz.boczkaj@pg.edu.pl (G. Boczkaj).

https://doi.org/10.1016/j.wri.2023.100230
Received 30 January 2023; Received in revised form 20 September 2023; Accepted 16 October 2023
Available online 2 November 2023

1. Introduction

Worldwide fresh water scarcity issues are increasing due to population growth and expansion of industrial development [1–5]. However, most of the water resources are comprised of saline water (between 30 and 50 mg/L). Thus, it is needed to develop prominent desalination techniques to convert saline water to pure water. To some extent, membrane and thermal based techniques are utilized at industrialized scale all around the world [1–3]; unfortunately, such systems own high energy expenditure and require skillful staff to operate high infrastructure units [5]. So, there is a need to get alternative but effectual systems in removing salts from saline water. CDI is an evolving technique that gained high attention as cost-effective, easy to operate and no secondary waste water technology [6–9]. Such systems are based on a pair of porous electrodes that are utilized to adsorb the ions during charging process, whereas the ionic species are liberated to restore the electrode through the discharging practice. Ionic species are detached from salty water by forming electrical double layers (EDLs) (Fig. 1a), in which the adsorbed charged ions are later desorbed either via short circuit, reverse potential or at zero voltage, as depicted in Fig. 1b. The intercalation of charged ions and/or redox reaction on oppositely charges electrodes as is illustrated in Fig. 1c.

To date, various carbon electrodes have been employed comprising activated carbon (AC) [10–12], mesoporous carbon [13–15], carbon nanotube (CNT) [16], carbon nanofiber [17,18] and reduced graphene oxide laminated and nanosheets [19], among many others. All these are sorted extensively as CDI electrodes owing to their porosity and good conductance [20,21]. Numerous studies have demonstrated that carbon-based electrodes possess excellent electrosorption capacity and selectivity for pollutants for instance, heavy metals, pesticides and dyes [22–25]. Peng et al. [26] produced TLPC2 electrode which demonstrated an excellent phosphate electro sorption capability of 231.56 mg/g with a rapid rate at 1.2 V. Mingming et al. [27] fabricated a bimetallic Zr–Al MOF-derived hierarchically porous ZAMC-13 electrode which exhibited exceptional phosphate electrosorption ability of 539.85 mg/g at 1 V. Though, carbon electrodes possess low deionization (salt removal) capability (15–25 mg/g) due to inadequate electrical double layers (EDL) formation and unavoidable side reactions such as carbon electrode oxidation and co-ion expulsion, which prevents carbon electrode utilization for CDI systems at high saline concentrations [28,29]. Recently, Sivasubramanian et al. [30] provided a brief review on CDI and electrosorption techniques with various electrode materials for the treatment of wastewater.

However, different CDI cell architectures which have been developed previously i.e. CDI, MCDI, desalination battery (or Faradaic deionization (FDI)) as depicted in Fig. 2, and another approach are to replace one of carbon electrode with sodium-ion insertion (SII) host substance [4,32], named as hybrid-capacitive deionization (HCDI) as depicted in Fig. 2d. It reveals a high salt removal ability than conventional CDI system [33–35]. Moreover, dual-ion intercalation electrochemical desalination (DEDI) (Fig. 2e), cation intercalation desalination (Fig. 2f) or sodium-ion desalination/cation desalination (NID & CID), and/or rocking-chair CDI (RCDI)) are additional architectures for the desalination battery using specific faradaic electrodes. DEDI makes use of different electrodes to specifically capture different ions. Details on the various materials used for faradaic electrodes can be found in excellent reviews focused on these aspects [9,29].

In CDI, desorption process lowers the efficiency and enhances the energy intake with counter-ions being simultaneously attracted to the electrodes. However, MCDI uses an ion-exchange membrane on each porous carbon electrode to prevent the so-called 'co-ion effect' [36]. It is generally believed that the intercalation type electrodes (FDI or desalination battery) do not require such a membrane due to their different desalination mechanism. Moreover, various CDI cell designs have been developed to further optimize the performance criteria as an optimal configuration can arise from electrode materials and architecture [37].

It is essential to acquire different types of substances employed for desalination and other related applications. SII host materials have shown great progress by introducing materials, for instance MnO_2 [38,39], Prussian blue and its analogues [40,41], $Na_2Ti_2(PO_4)_3$ (NTP) [42–44], $Na_3V_2(PO_4)_3$ [45], etc. In 2011, a novel kind of two-dimensional (2D) material like transition metal carbides and

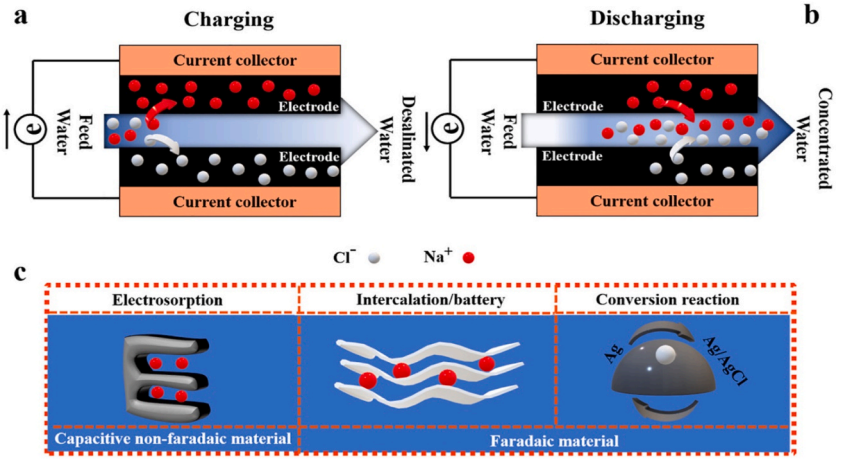

Fig. 1. CDI concept, a) charging process, b) discharging process, and c) model of ions elimination procedure through diverse electrode kinds. Reprinted from Ref. [31] copyright (2020), with permission from Elsevier.

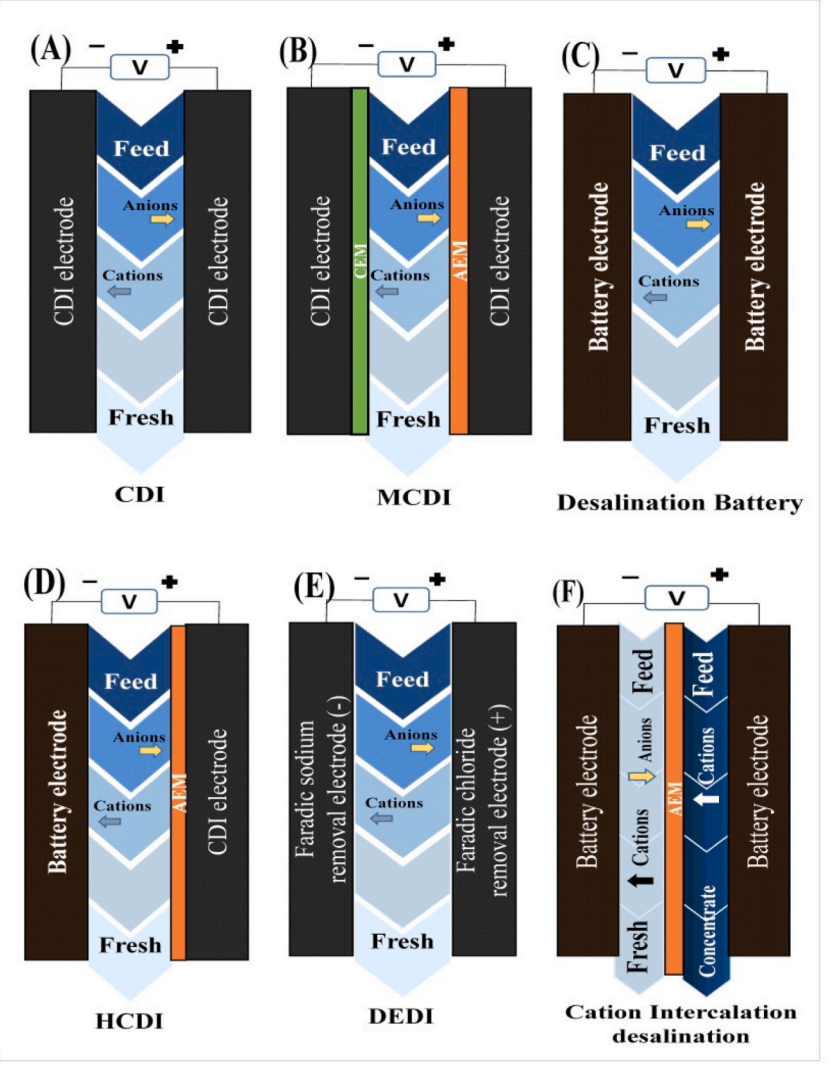

Fig. 2. Schematic showing CDI cell designs: (A) conventional CDI, (B) MCDI which involves the use of ion-exchange membranes, (C) desalination battery or FDI makes use of faradaic intercalation electrodes, (D) HCDI with the use of an anion exchange membrane (AEM), (E) dual-ion intercalation electrochemical desalination (DEDI). And. (F) Cation intercalation desalination also known as RCDI or (NID&CID) with the utilization of an AEM [37].

nitride compounds, known as MXene, have been informed [46]. MXene has exhibited competitiveness in desalination and energy storage fields because of 1) exceptional layered structure, 2) excellent conductance, 3) high surface area, 4) chemical steadiness and 5) mechanical properties [47,48].

MXenes are rapidly developing materials that basically are created from MAX phases. MAX phase is ternary transition metal's big group; carbides and nitrides having formula of $M_{n+1}AX_n$, here n is ¼, 1, 2, or 3, M is first transition metal i.e., (Ti, Cr, Nb etc.), A belongs to IIIA or IVA group elements (Al, Si, etc.), and X is C and/or N [49]. A schematic diagram related to MAX and MXenes is shown in Fig. 3.Where, the MAX phase is an alternate structure of MX and MA layer. Herein, MX layer is mainly covalent and ionic bonds, while MA layer is a metal bond. The binding force of attraction between MX layers is higher than the MA layer and offers probability to remove A from MAX phase. After A layer removal from MAX phase, the MX layer connects freely with surface termination groups i.e., O^{-}, F^{-}, or OH^{-} referred as T in a $M_{n+1}X_nT_x$ formula [51]. The etching is required for MA elements, where bonds are strong enough to make the mechanical delamination unattainable. MAX phases etching procedures include HF-etching [52,53] and its etchant are LiF/HCl KCl/HF combinations [54] or NH_4HF_2, NH_4F [55,56] and NaOH etchant [56]. The electrochemical approaches can also be employed to change MAX phases to MXene [57]. Furthermore, different forms of MXene are obtained through diverse fabrication methods, such as hydrogel [58], film [59] and powder. MXene interlayer spacing and termination groups are dependent on different etching approaches [59]. The interlayer water molecules and terminal functional groups influence the MXene electrochemical capacitance [53]. During the etching practice dissociation of cations occurs, where cations and H_2O molecules get intercalated in MX

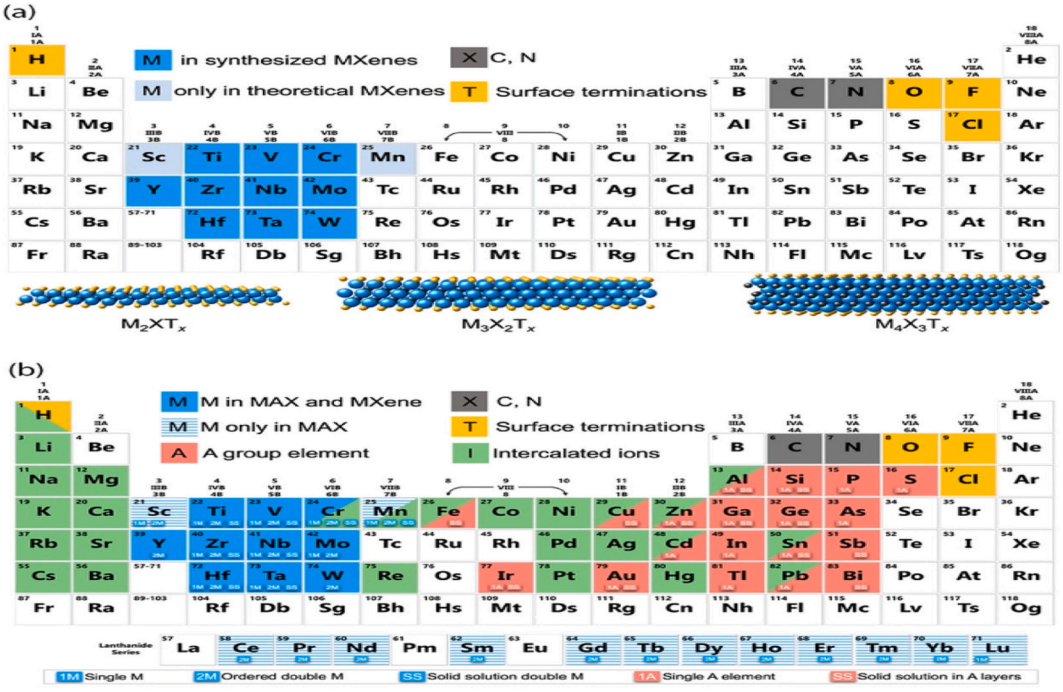

Fig. 3. Periodic tables presenting configurations of MXenes and MAX phases. (a) Elements used for MXenes synthesis. (b) Elements used to yield MAX stages, MXenes, and their intercalated ions. Detailed description is available in source publication. Reprinted from Ref. [50] copyright (2019), with permission from Elsevier.

layers in order to get large spacing TiC_2T_x materials and after minor oscillations, single or multilayered TiC_2T_x MXene is prepared. Thus, etching approaches mainly effect on electrochemical functioning of MXene and almost all the MXene-derived CDI electrodes are prepared via the HF-etching process.

Plenty of research works have been achieved for the MXene compositions [53,60,61], of which Ti_3AlC_2 is suggested as one of the most extensively investigated agent [62]. Ti_3C_2 MXene substance is attained by etching Al atom layer from Ti_3AlC_2 with hydrofluoric acid (HF) [46,63]. Due to removal of Al, conductivity of precursor material is decreased [46,64]. Similar to all two-dimensional materials, these too yield stacked layer and create dense structure while electrodes preparation process due to layer interaction, that significantly affect surface area and ionic species transmission inadequacy cause low efficiency of these prepared MXene electrodes. These drawbacks are overcome through mixing TiC_2T_x MXene with zero, one and two-dimensional materials [65]. Layers of MXene material are treated with different substances, such as activated carbon [66,67], metal oxide particles [68], carbon nanotubes [66,69] and polymer substances [70–72]. These synthesized composite materials achieve high capacitive properties, but volume capacitance certainly reduces as a result of density decrease caused by open space.

Nevertheless, MXene materials are under major investigation nowadays to develop advance materials [73]. These features include high surface area (347 m^2/g), eco-friendliness, activated metallic hydroxide sites, biocompatibility, facilitate functionalization, antibacterial property, hydrophilic nature, good metallic conductivity make it a perfect candidate for several applications; for instance, energy storage devices, electronics, environmental remediation, sensors, and catalysis [74–77]. MXenes own exceptional conductivity and high surface area which makes it significant for energy storage, conductive films, adsorption and electrical measurements [74,78]. Recently, MXenes are also utilized for water splitting and water treatment, i.e., capacitive deionization and membranes [79–84].

So far, several different types of electrodes that have been utilized in CDI have their peculiar benefits and features; AC electrodes are economical and versatile but lack of best conductivity and specific selectivity. CNT electrodes have great conductivity and surface area (SA), which improve ion kinetics, but they could be costly to produce on a big scale. Graphene electrodes, which have high mechanical strength and conductivity, have the same problems but may be more versatile. Metal oxide and polymer electrodes can both give adapted selectivity, but their production is complicated.

MXene-based CDI electrodes have a number of advantages over other kinds of electrodes. Employing their 2D structure, MXene-based CDI electrodes deliver substantial SA and quick ion adsorption owing to superior conductivity. The functionalization of their selectivity and tunability advances ion removal, and the mechanical stability confirms continued usage. Moreover, MXene has many advantages over traditional electrodes, exclusively in terms of their capacity to go beyond the concentration polarization limitation and offer low-energy solutions for brackish and seawaters [85].

A number of reviews have been published to explore the current state of the art for various MXene-based electrode kinds and their mechanisms. Zhang et al. [29] compared MXene's present endeavors in the larger domain of faradaic and HCDI to those of other materials and with numerous architectures in order to detect the research gaps in the utilization of MXene for these uses. Fuhar et al.

[85] presented a contemporary review of MXenes and MXene-composites' applications in desalination and water treatment. The influence of water components and operating conditions, in addition to an investigation of the kinetics and isotherms, were also covered. Furthermore, in our previous review [86], we discussed MXene-based water treatment materials and the applications of MXene-based membranes adsorbents and photo-catalysts in removing antibiotics and heavy metals from water. Also comparison of MXene-based membranes with other 2D membranes was outlined.

Keeping in view the fast-moving progress, we focus on most recently synthesized MXenes, and its composites implemented in CDI applications. Few-layer MXene (FL-MXene) and multilayer MXene (ML-MXene) structures are formed when as-synthesized MXenes are etched through various candidates (ML-MXene). We begin with electrochemical energy storage mechanisms, then go on to MX synthesis. After that, we briefly review the synthesis approaches of MXene composites made for CDI technology.

2. Principles of electrochemical energy storage mechanism

CDI is based on the electrochemical capacitors mechanism also known as electrical double layer capacitor (EDLC) due to its principal charge storage process. Electric devices accumulate charges either via one or mechanisms combination, as shown in Fig. 1 (EDL, Faradaic, Intercalation). EDL storage develops directional electrostatic interactions at the electrode interface and electrolytes. The counter-ions in electrolyte solution progress towards adsorbed ions to sustain charge neutrality. Though, with increasing distance from electrode, charges accumulation decreases exponentially as described by Gouy-Chapman theory [87], as shown in Fig. 1c. EDL adsorption mechanism depends on two factors i.e., electrode morphology and electrolyte type [88]. Thus, materials, which possess high surface area to volume relation, exhibits highly established EDL interfaces [88] and EDL charge storage may be described as a surface phenomenon. However, EDL-based traditional CDI system has some drawbacks, including a low deionization capacity, an excessive co-ion expulsion, a poor cycle life, a low physical storage capacity, and parasitic reactions [89].

To overcome the limitations of the capacitive electrosorption in carbon based CDI electrode materials, the capacity of material to store higher amounts of ionic species can be improved through Faradaic or redox reaction (see Fig. 1c). Faradaic electrodes which store ions via pseudo capacitive mechanism have been proposed [90]. The pseudocapacitive mechanism can either be redox or intercalation in nature. Redox pseudo capacitive mechanism occurs when ions are adsorbed electrochemically at/or near the electrode surface accompanied by electron charge-transfer at the interface between electrolyte and the electrode [91]. Functional groups play key role in electrochemical activity of materials. Electron charge transfer at the electrode/electrolyte interface creates dynamic double layer development. The charge transfer is fast and dynamic, and no chemical reaction occur at electrode surface. Faradaic charge storage (pseudo capacitance) happens in combination with EDL storage and changed through oxygenated functionalities and ionic species attraction towards electrode plane. Moreover, Faradaic reactions can produce hydroxide (OH^-) ions in an aqueous environment and trigger overall capacitance by hydrogen bonding storage.

Additionally, intercalation process (see Fig. 1c) is different from former two mechanisms. In pseudocapacitive intercalation majority of electrode substance contributes in charged ions accumulation instead of electrode plan i.e., ions are stored in the lattice sites of the intercalation host compounds (IHCs) where electron charge-transfer take place without changing the phase of the material [91]. It is reversal insertion of ionic species or molecules in between layered materials spacing. Intercalation charge storage devices development is still in investigation and progress phase. Scientists are strongly focused on the developments of layered crystal structure material which has capability to rapid 2D transport paths. Ion's intercalation in surface sensitive films, along with redox active substances, can permit all three mechanisms to work instantaneously. Thus, indicating to charge storage devices which assure high energy density, power density and extensive cyclability [92].

3. Synthesis routes for MXene

In 2004, graphene separation was discovered [93], since than the domain of 2D and layered materials have developed rapidly [94]. Recently, significant number of 2D-materials have been revealed and investigated, for instance MoS_2, borophene, black phosphorous, hexagonal boron nitride (hBN), silicone, transition metal dichalcogenides (TMDs) and MXene [92].

MXene has been synthesized by chemically etching its specific precursors. Though, etchants are separated into two types, 1) Acidic solution comprising fluoride ions (HF, LiF/HCl, or NH_4HF_2), and 2) salts containing fluoride ions (NH_3, KF, LiF, or NaF). Primarily, MXenes are detached from MAX stages through saturating MAX stages in certain acids and breaking the M–A bonds, while this procedure, specific corrosion time and complete agitation are required. Naquib et al. produced first time MXene, TiC_2T_x, via etching Ti_3AlC_2 utilizing 50 % concentrated hydrofluoric acid (HF) to produce Ti_3C_2 MXenes at ambient temperature for 2 h [46]. Thus, HF-etching approach is effectively employed to other MAX phases and generating numerous novel MXene substances such as, Ti_2CT_x [95], V_2CT_x [61,96], Nb_2CT_x [61], Ti_2NT_x [97], $(V_{0.5}Cr_{0.5})_3C_2T_x$ [96], $(Ti_{0.5}Nb_{0.5})_2CT_x$ [64], $Mo_{4/3}CT_x$ [98], $Nb_{4/3}CT_x$ [99], $W_{4/3}CT_x$ [100], $Ti_3C_2T_x$ [101,102], Ti_3CNT_x [64], $Ta_4C_3T_x$ [64], $V_4C_3T_x$ [103], $Mo_2TiC_2T_x$ [104], $Mo_2Ti_2C_3T_x$ [55], and $Cr_2TiC_2T_x$ [104]. Later, Ghidiu et al. developed an alternate method due to harmful effect HF on human beings and environment, they utilized safer solution mixture of HF, HCl and lithium fluoride (LiF), where Ti_3AlC_2 materials were saturated at 35 °C for 24 h to achieve $Ti_3C_2T_x$ [56]. Likewise, HCl and LiF combination solution has H^+ and F^- ions, following the similar etching process for MAX steps with HF solution. However, other acids and ionic compounds, comprising fluorine ions (NaF, FeF_3, KF, CsF, CaF_2) mixtures, have been utilized for MXenes synthesis [54] and successfully synthesized MXenes containing Ti_2CT_x, Mo_2CT_x [105], V_2CT_x [106], $W_{4/3}CT_x$ [100], $Ti_3C_2T_x$ [54], Ti_3CNT_x [107], $Cr_2TiC_2T_x$ [104] and $(Nb_{0.8}Zr_{0.2})_4C_3T_x$ [108]. Still, these etching methods liberate few harmful gases. Afterward, Hliam et al. developed another approach without producing harmful gases when using weak acidic and eco-friendly fluoride comprising NH_4HF_2 that can produce MXene material [109]. Feng et al. achieved another approach and observed that surface

functionalities presence generates $Ti_3C_2T_x$ plane negative, which cause the attraction of cations towards its surface and lattice factor of $Ti_3C_2T_x$ is increased accordingly [110]. Urbankowski et al. synthesized nitride-based MXene through heating a $TiAlN_3$ mixture and molten fluoride salts [111]. This gave good demonstration of 2D transition metal nitrides. Additionally, novel group of ternary and quaternary materials with $MnAl_3C_2$ or Mn $[Al(Si)]_4C_3$ formulae may be utilized to produce MXene beside MAX phases [112] and they have successfully prepared Zr_3CT_x and $Hf_3C_2T_x$ compounds. Fig. 4 displays the common production process for all these considered ways, demonstrating the utmost traditional etching and intercalation agents.

Additionally, after their synthesis, MXenes are formed as a multi-layered material, requiring further processing to obtain a single-layered material. There are two approaches to delaminate multi-layered MXenes, such as mechanical delamination and delamination by intercalation (see Fig. 3). In mechanical delamination, very low monolayer MXenes are obtained due to strong bond interaction of multi-layered MXenes. Few research works have done through mechanical delamination [81,113]. Intercalation is most widely used for single layered flakes synthesis, as there is space between multi-layered MXenes which can hold charged species. This interlayer space can be enhanced via intercalation. Hence, intercalated MXene substance can be transferred into separate films through sonication in deaerated water [114]. Furthermore, there are two kinds of intercalants: 1) organic compounds, and 2) ionic compounds. The synthesized MXenes via HF-etchant requires organic intercalant compounds, generally contain polar molecules for instance, urea, isopropyl amine, hydrazine etc. For multi-layered MXenes produced via Li^+ or NH_4^+ ions from LiF + HCl or NH_4F etchant can insert among layers of MXene. Thus, larger c lattice parameters of MXenes are obtained than using HF-etchant [115].

4. Advent and progress of MXene-based electrodes in CDI

Innovative MXene compounds have recently been formed in order to generate stable and multifunctional electrode substances. MXene is a significant option for the making of multifunctional composites because of its 2D structure, layered morphology, and good flexibility. Owing to its electrical conductivity, hydrophilic nature and flexibility, MXene-based CDI electrodes have displayed exceptional adsorption capability [117,118]. By putting Ti_3C_2 onto the permeable separator of a CDI unit, Srimuk et al. [117] produced the first MXene-based electrode. The electrodes' salt removal capacity (SAC) was determined to be 13 mg/g at 1.2 V and had an excessive cyclability of roughly 30 cycles but charged species adsorption was observed via intercalation rather than EDL development.

Despite the significant advancements made to MXene-based CDI techniques to date, the simply stacked property resulting from weak van der Waals attractions between sheets has proven a restriction to further advancement. To face this concern, Vacuum freeze drying was the approach worked by Bao et al. to create porous MXene [119]. The restacking of MXene nanosheets can be reduced with this behavior. Therefore, the electrolyte's accessibility in the pores is enhanced, favoring an increase in overall capacitance. Moreover, the porous $Ti_3C_2T_x$ structure generates a 3D network, which offers the ions with a multidimensional ion diffusion passage. The porous $Ti_3C_2T_x$ MXene electrode confirmed 118 mg/cm^3 SAC in a 10,000 mg/L NaCl solution at 1.2 V when exposed to desalination. Knowing that MXene has a very negatively charged exterior with –OH, –O, and –F functionalities, it could be used as a cationic selective cathode material to reduce co-ion impaction. Though, HF-etched MXene undergoes from an excessive ion diffusion difficulty and inability to accommodate more ion because of the small interlayer gaps. Cations are effortlessly and freely intercalated into MXene in alkaline solution, which favors widening the interlayer gap and activating the passage of ionic species. Also, the interlayer spacing of $Ti_3C_2T_x$ improved from 9.8 to 12.1 Å after NaOH handling, which is advantageous for sodium ion diffusion and storage between the layers [120].

Hence, consider that self-restacking diminishes the active electrochemical sites' exposure. Thus, increasing the interlayer gap of $Ti_3C_2T_x$ flakes with intercalating compounds (water, cations, DMSO, and other intercalants) has proven to be a vital step in decreasing the interaction (van der Waals attraction) between 2D films and delaminating MXene into distinct layer [121]. A right solvent is necessary for the intercalation and delamination process, a mixing stage in which the intercalant is inserted between 2D films, an

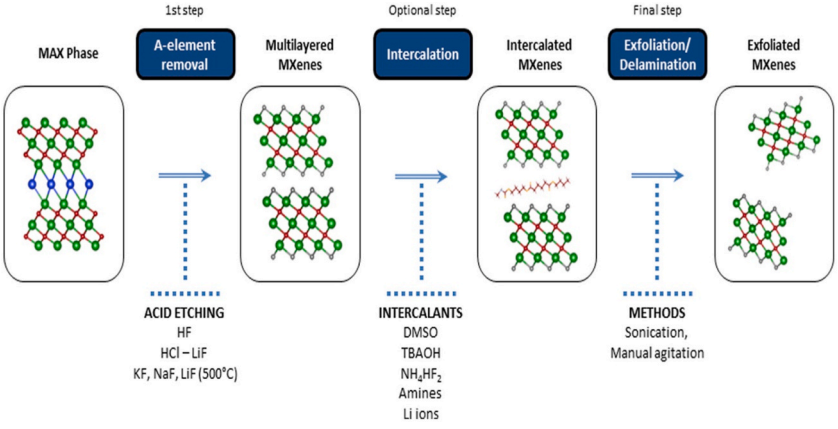

Fig. 4. MXenes manufacture approach representation. By utilizing MAX stage etching with acidic solutions, the metallic "A" element is removed (e.g., Al). The attained multi-layered complex is exfoliated via mechanical or manual agitation in order to acquire a few MXenes films. To quicken the exfoliation, an intercalation step may be utilized. Reprinted from Ref. [116] copyright (2019), with permission from Elsevier.

infrequent sonication stage altering on preferred flake range and quantity, and a centrifugation stage to segregate the delaminated substance from the multilayered material (nondelaminated) [114]. The resulting colloidal suspension will comprise scattered 2D layers of electrostatically steadied MXene that are firm against accumulation, clumping, and processing. Furthermore, the sonication stage is greatly reliant on the etching process and appliance, along with the concentration necessitated. Sonicating for extended time and at greater momentum will result in reduced flakes with extra flaws, as well as quantities that differ from non-sonicated samples. The MXene sheets quantity in solution is induced via a variety of reasons, counting the production processes and intercalants employed to reduce the interlayer connection between MXene sheets.

On the other hand, poor conductivities and hydrophilicities were found in most intercalation agents than $Ti_3C_2T_x$ MXene, lowering the composite's conductivity and making the electrolyte ions less accessible, affecting rate capacity and cycle steadiness. Interestingly, MXene is very hydrophilic with strong conductivity and an open two-dimensional structure that allows electrolyte ions to enter and electrons to flow quickly during charge and discharge processes. Shen et al. [122] also presented an easy but applicable method for regulating the $Ti_3C_2T_x$ material dimensions they produced. To make all-MXene-based electrodes for HCDI, they used $Ti_3C_2T_x$ nano-sheets as both an intercalateng agent and an active material. Since all-MXene electrodes have superior electrical and ion availabilities, they displayed an excessive electro adsorption capability of 72 mg NaCl/g L-*S*-$Ti_3C_2T_x$ and outstanding cycling steadiness, highlighting the favorable capacity of all-MXene electrodes for salt removal uses. As a result, it is significant to maximize the essential fundamental benefits of 2D-MXene materials, such as enhanced interlayer gaps and stable sodium ionic species transport passages. For intercalation-type Ti_3C_2 electrodes, a greater interlayer gap can usually give additional ion storage area. More importantly, greater interlayer spacings can efficiently boost electrosorption's reversible capacity. The literature says that certain confined Na^+ ions are utilized as a sodium column to alleviate the stable interlayer gap in the practice of adsorbing Na^+ ions in order to reach quick reversible adsorption and desorption as the interlayer spacing is a limitation [123]. Consequently, figuring out how to construct an MXene electrode with a larger interlamellar distance remains a pressing issue. Inserting an interlayer medium is a simple and successful method which has been examined to avoid the accumulation and re-stacking of 2D-nanosheets and enhance the interlayer gaps of 2D nanomaterials [124,125]. Chen et al. [126] used a sequence of altered processes of molten-salt produced Ti_3AlC_2 and NaOH usage to make $Ti_3C_2T_x$ with sub-size particles and enlarged interlayer space. The sub-size and Na^+-intercalated $Ti_3C_2T_x$ was employed as CDI cathode electrode. In a 100 mg/L NaCl solution, the Na^+-$Ti_3C_2T_x$-MS exhibited good CDI operation, with a high electro sorption capability of 14.8 mg/g, an excessive charge efficiency of 0.81, and strong cycle constancy at 1.2 V. Overall, this research introduced an innovative model strategy for intercalation-type CDI electrodes.

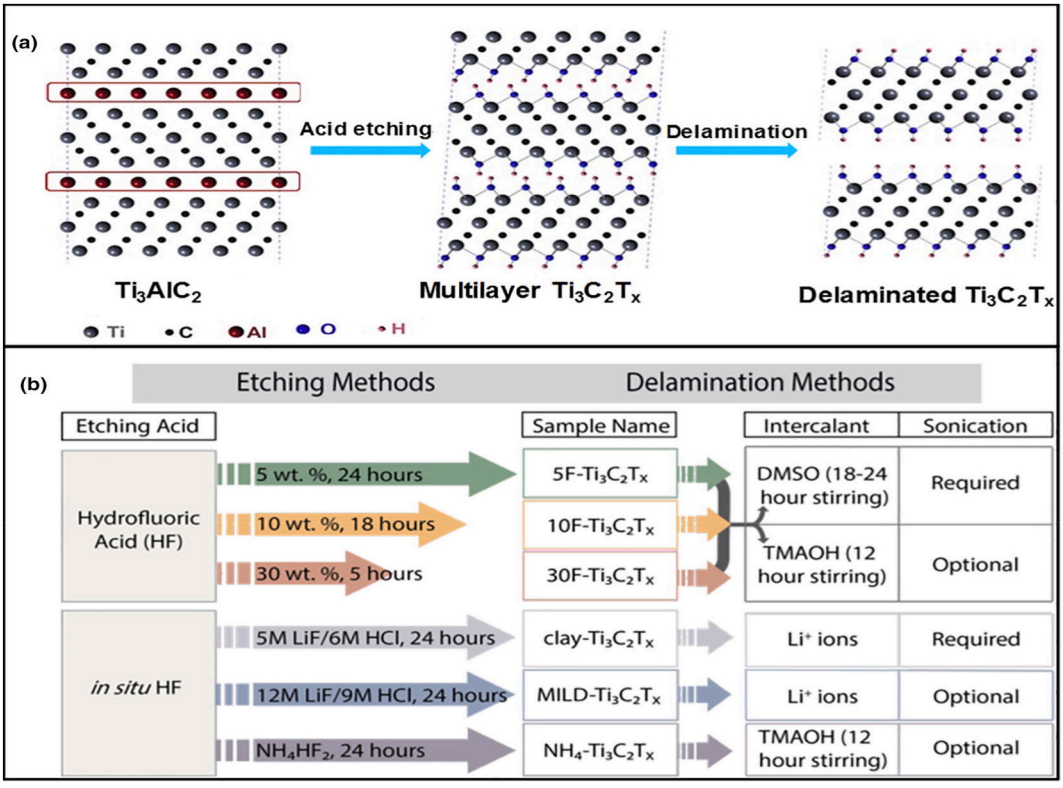

Fig. 5. (A) The modifications in atomic arrangement of Ti_3AlC_2 through the exfoliation practice from the MAX stage precursor (Ti_3AlC) to ML-$Ti_3C_2T_x$ and lastly DL-$Ti_3C_2T_x$ post sonication/cation intercalation, (b) Manufacture methods for the preparation of DL $Ti_3C_2T_x$ employing direct HF and in situ HF approaches Reprinted from Ref. [73] copyright (2019), with permission from Elsevier.

Furthermore, subsequent sonication, the layers can be mechanically separated to create delaminated (DL) $Ti_3C_2T_x$ (DL-MXene) suspensions (Fig. 5a). Whereas, in Fig. 5b, a diagram depicting the configuration and production paths of MXenes at ambient temperature, employing straight HF or in situ HF, in addition to multiple ML-MXene delamination paths are given. The HF concentration and the reaction time disturb the etching of Al films by the direct HF procedure [55,127,128].

The $Ti_3C_2T_x$ electrode was made by Shen et al. [129] via mixing 0.2 g of multilayer $Ti_3C_2T_x$ with 18 mL of a DMSO (dimethyl sulfoxide, 99 %) solution, after then, a delamination reaction took place at ambient temperature for extra 18 h. The delaminated $Ti_3C_2T_x$ was then removed from the DMSO solution via centrifuging the colloidal solution for 1 h at 9000 rpm. The delaminated $Ti_3C_2T_x$ was dispersed in DI water after decanting the supernatant. This dispersion was utilized as the preliminary diffusion to make

Table 1
Outline of the desalination operation of different MXene//AC electrodes composites.

S. No	Electrode Material	Electrosorption capacity (mg/g)	Voltage (V)	Charge efficiency (%)	Stability (cycles)	Specific capacitance (F/g)	Remarks	Reference
1	AC//3D-Na^+-$Ti_3C_2T_x$	16.2	1.2	81	10 (94.4 % remaining electrosorption capacity)	143.2	3D-Na^+-Ti_3C_2Tx was synthesized through NaOH-induced crushing of the $Ti_3C_2T_x$ nanosheets. The connected $Ti_3C_2T_x$ sheets produce a 3D system arrangement and considerably improve the conductivity. This work enhanced the CDI working of MXene electrode: change of 2D film structure into 3D spongy nets. Though, the oxidation of $Ti_3C_2T_x$ in aqueous solution reduced its CDI functioning.	[131]
2	CNT/ $NaMnO_2$// AC	32.7	1.2	65	100	189.5	The authors investigated the two-layered MnO_2-based nanomaterials as HCDI redox-active intercalation electrodes with extended interlayer spacing and an open porous structure. The Na^+ ions migrated easily to the active sites owing to the short ion diffusion channel provided by the as-acquired $NaMnO_2$, which has an exposed porous configuration. Furthermore, both materials revealed remarkable reproducibility and great initial ion removal capabilities.	[132]
3	MXene-CNT//AC	12	1.2	85	100	123	The electrochemical act of asymmetric HCDI utilizing MXene-CNT coupled with AC for electro sorption of low and high NaCl solutions were examined. The studies revealed that MXene-CNT combined with activated carbon can remediate aqueous 600 mM NaCl without the necessity for an ion-exchange membrane, despite having slightly lower charge efficiency and desalination ability. The removal of the ion-exchange membrane from the unit constituents might therefore notably lower the whole expenses in light of trade uses.	[133]
4	Ti_3C_2//AC	26.8	1.2	–	–	–	The interlayer space for the MXenes $Ti_3C_2T_x$ is capable to be enhanced for effective Na^+ ion passage via Ar plasma. Similarly, electrochemical investigation showed an advanced volumetric and gravimetric capacitance for MXene $Ti_3C_2T_x$ as of the inferior innate resistance.	[134]

multiple dispersions that remained sonicated for 1 and 2 h to yield identical mixtures with varying sized scales. The steady dark green supernatant was composed after centrifugation of 1 h. Further 1 h of centrifugation at 3500 rpm, the residue was re-dispersed in DI water and the large-size (L-$Ti_3C_2T_x$) MXene was recovered. Small-size (*S*–$Ti_3C_2T_x$) MXene permanent dark green supernatant was recovered following 1 h of centrifugation at 8000 rpm, followed by sonication for 2 h. The L-*S*-$Ti_3C_2T_x$ flakes were made by mixing a dispersion with the equal overall mass of L-$Ti_3C_2T_x$ and *S*–$Ti_3C_2T_x$ films. Nylon membrane vacuum filters were used to filter the three colloidal solutions. The freestanding L-$Ti_3C_2T_x$, *S*–$Ti_3C_2T_x$, and L-*S*-$Ti_3C_2T_x$ flakes were simply stripped off the membrane after air drying at ambient temperature. The free-standing MXene layers were trimmed to a magnitude of 1 × 1 cm for the electrochemical extent, and a membrane with a diameter of 40 mm was employed for HCDI to make the $Ti_3C_2T_x$ electrodes. Without any binders, MXene layers were employed directly as electrodes. There prepared electrodes exhibited excellent electro sorption capacity about 72 mg/g with outstanding capacitance 169 F/g.

4.1. MXene/activated carbon electrodes

According to numerous studies, MXene has a great pseudo capacitance that outperforms the energy storage capabilities of the majority of other capacitive substances, mainly when standardized to the electrode dimensions. The capability to create electrodes without a binder (MXene paper) and to act as a nearly perfect intercalation substance with speedy ion inclusion between the MXene films is what sorts MXene so unusual.

Srimuk et al. [117] employed the traditional way of etching ternary titanium aluminium carbide, or the MAX part (Ti_3AlC_2), with HCl, they made Ti_3C_2-MXene. Without the addition of a binder, the MXene material was pasted right onto the porous separator of the CDI unit and revealed very steady functioning around 30 CDI sets with an average SAC of 13 ± 2 mg/g and exhibited capacitance value of 132 F/g. Interestingly, vacuum freeze drying, replacing HF etching and nitrogen doping, was all accomplished. These replacements were applied to avoid MXene layers from restacking and produce an electrochemically active porous substance, and these studies exposed MXene to be an auspicious material for salt removal [130], some MXene composites materials have been investigated as well, as shown in Table 1. Furthermore, Chen et al. [130] intercalated Na^+ with $Ti_3C_2T_x$ (NaOH–$Ti_3C_2T_x$) and used as cation-selective cathode in HCDI and AC was used as anode. An easy method was utilized to produce NaOH–$Ti_3C_2T_x$ as shown in Fig. 6a.

The salt removal capacity of asymmetric AC//NaOH–$Ti_3C_2T_x$ (Fig. 6b) compared to symmetric (AC//AC) electrodes were 12.19 and 4.55 mg/g, respectively [130]. Furthermore, in the desalination mechanism of asymmetric CDI cell the charge efficiency and adsorption capability could be ascribed to the cathode which can attain cation selectivity, adsorption of Na^+ ions via intercalation and rejection of Cl^- ions throughout electrostatic repulsion to considerably reduce the co-ion removal consequence. Moreover, the NaOH treatment increased interlayer space of $Ti_3C_2T_x$ from 9.8 to 12.1 Å, thus could facilitate the diffusion and storage of Na^+ ions between

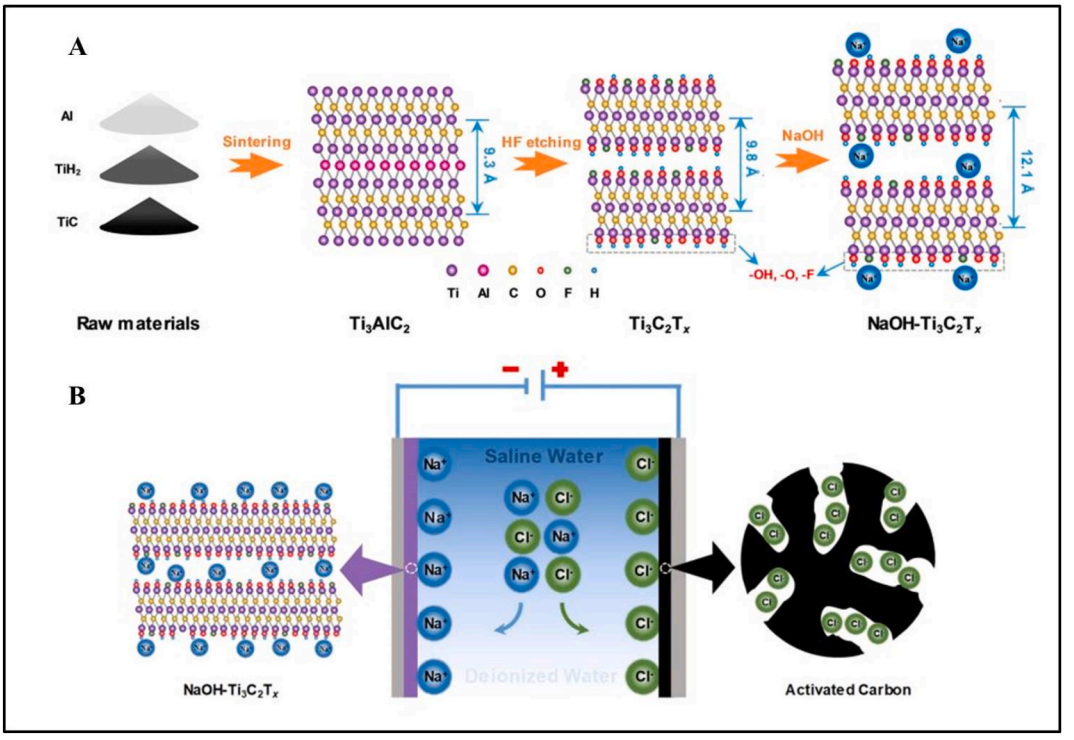

Fig. 6. (A) Synthesis practices of NaOH–Ti_3C_2Tx and (b) asymmetric CDI cell (AC//NaOH $Ti_3C_2T_x$). Reprinted with permission from Ref. [130]. Copyright (2020), American Chemical Society.

the layers. Thus, MXene presents exceptional ability as a cation-selective cathode material with decent cyclic steadiness in asymmetric CDI.

Additionally, a novel asymmetric CDI arrangement was formed using date-seed derived carbon (DSAC) and MAX (Ti_3AlC_2) as an anode and cathode respectively [135]. The facile strategy was used for the pyrolysis of DSAC. FE-SEM was utilized to discover the morphological and topological properties of these electrodes at different magnifications. DSAC showed a characteristic honeycomb-like form made up of porous 3D linked carbon walls, as viewed in Fig. 7 (a and b). FE-SEM pictures of commercially accessible Ti_3AlC_2 (MAX) with a layered flake-like microstructure and a normal particle size of 2–5 μm are presented in Fig. 7 (c and d). Moreover, the produced Ti_3AlC_2 can be applied to enhance the interlayer spacing between the metal carbide structures by 10 min sonication in NMP mixture (see Fig. 7e). Additionally, the observed substance was investigated through EDS to validate the structure of exfoliated MAX, and the ensuing spectrum is displayed in Fig. 7f. It is certain that the exfoliated MAX involves Ti, C, and Al, demonstrating that the sample's arrangement was unchanged via by NMP sonication.

The SAC summaries of the DSAC/MAX electrodes are also depicted in Fig. 8 (a and b) at several applied voltages and influent Cr ($_{VI}$) concentrations. The applied voltage effects are represented in Fig. 8a. Due to improved electrochemical redox performance, the highest SAC of 38.6 mg/g was attained at 1.2–1.4 V. Besides, as displayed in Fig. 8b, the SAC of electrodes has an obvious association with the amount of Cr ($_{VI}$). Enhancing the Cr ($_{VI}$) strength from 40 to 120 mg/L can support EDLs build up in DSAC micropores and boost the convenience of MAX's redox sites. At 1.2 and −1.2 V potentials difference, the asymmetric DSAC/MAX electrodes recyclability was explored over the progression of two cycles. The renewal behavior of the DSAC/MAX electrodes is displayed in Fig. c. This asymmetric CDI classification was restored and reused efficiently. Fig. 8d illustrates 10 sorption cycles for the DSAC/MAX electrodes, where the SAC of these electrodes declines after 10 cycles, with just 58 % of the preliminary SAC remaining. Furthermore, Fig. 8 (e and f) demonstrates the complete CDI experimental setup along with a plausible adsorption procedure. ICP-MS was utilized to investigate the electrochemical conversion of $Cr_{(VI)}$ to $Cr_{(III)}$ on the electrode exterior [136]. Fig. 8f depicts a probable systematic method to Cr($_{VI}$) decline and adsorption on the asymmetric DSAC//MAX conductors [135].

Additionally, water electrolysis at the DSAC electrode formed enough H^+ ions to decrease Cr ($_{VI}$) ions. While electrochemical redox change of Cr ($_{VI}$) to Cr ($_{III}$) ions was noticed at Ti_3AlC_2 stacked multilayers. The capacitances of DSAC and MAX were 250 and 347 F/g, correspondingly. The CDI functioning of these electrodes was good, with adsorption capability of 38.9 mg/g at 1.2 V. As a result, these asymmetric electrodes indicate a high-performance CDI system capable of powerfully eliminating hazardous metals from industrial waste.

4.2. MXene/oxide electrodes

MXene-oxide composites are prospective supercapacitors materials, Na^+ or Li^+ ion batteries in consequence of their exceptional conductance and decent firmness [137] and desalination. Exceptional physicochemical features of 2D metal oxide nanosheets with high SSA have demonstrated extensive investigation curiosity in the power-storage area. For Na^+ ion batteries, MnO_2 nanosheets inserted with Li^+ family ions, acting as a cathode substance, has revealed outstanding performance [138]. As a result of this, MnO_2 nanosheets as an electrode can be employed to improve CDI running even more. More crucially, 2D MnO_2 nanosheets can self-assemble into a 3D open porous structure, improving material utilization and ensuing in high intercalation and ion removal competences [138]. Byles et al. applied binary layered manganese oxides (LMOs) as HCDI probes for the elimination of charged species from NaCl and $MgCl_2$ solutions, with sodium (Nabirnessite) and magnesium (Mg-buserite) ions stabilizing the interlayer area, with extraordinary HCDI performance [39]. In addition, amorphous MnO_2 was utilized to modify CA electrodes through CV and electroless deposition (ED). The relation between oxide covering morphology, electrode conductivity, and Na^+ elimination efficiency was investigated via MnO_2-coated CA electrodes for CDI performance. Though, both deposition practices boosted electrode capacitance, only ED electrodes outperformed bare aerogels in terms of desalination, attaining an extreme of 0.77 mmol-Na^+/gram of cathode [139]. Liu et al. [140]

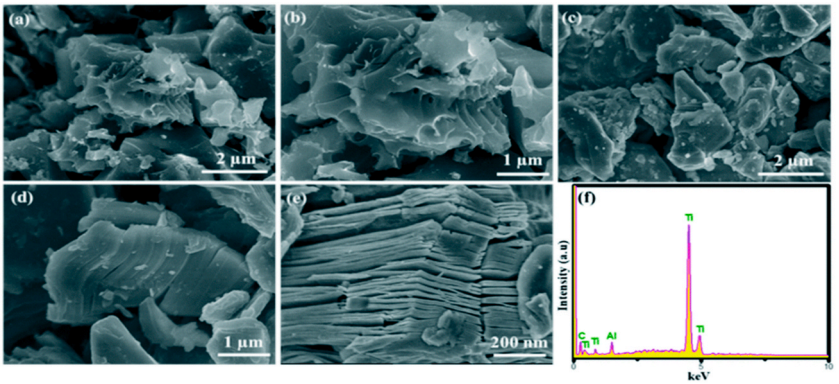

Fig. 7. DSAC produced from date seed waste biomass through one phase pyrolysis at 800 °C for 4 h in N2 conditions, revealed in diagrams a and b via FE-SEM investigation; (c–e) FE-SEM study of commercial MAX (Ti_3AlC_2) and samples prepared via enhanced sonication (10 min) and at ambient temperature; (f) sonicated MAX (Ti_3AlC_2) EDS spectrum. Reproduced from Ref. [135] copyright (2020), with permission from Elsevier.

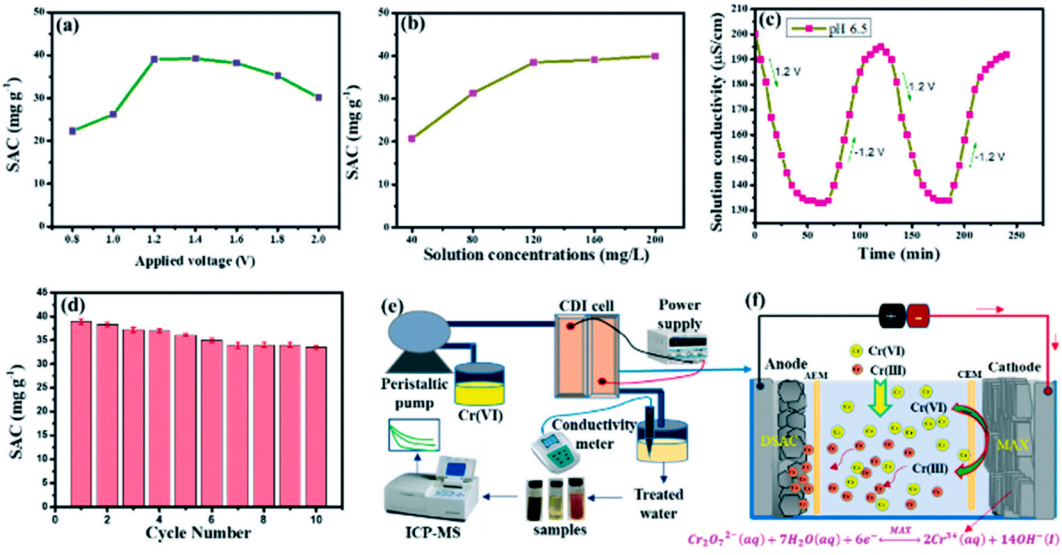

Fig. 8. (A) Given voltage vs. SAC, (b) solution strength vs. SAC, (c) restoration outline with two successive cycles, (d) 10 repeated renewal rounds vs. SAC of the DSAC//MAX electrodes at pH 6.5; (e) CDI system chart and (f) the mechanism concerned in $Cr(_{VI})$ reduction by DSAC//MAX conductors. Republished from Ref. [135] copyright (2020), with permission from Elsevier.

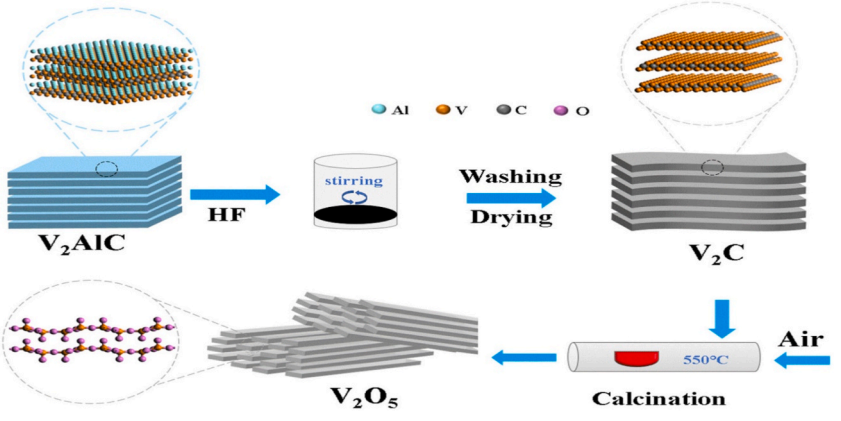

Fig. 9. Illustration for the formulation of V_2O_5. Reproduced from Ref. [126] copyright (2021), with permission from Elsevier.

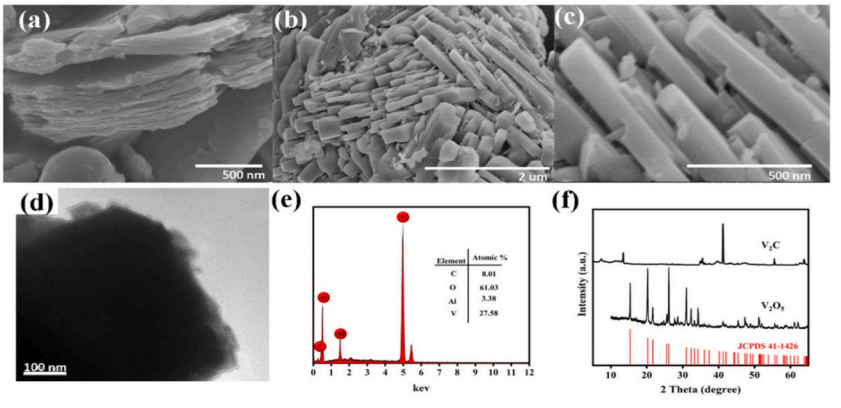

Fig. 10. (A) V_2C SEM pictures, (b, c) SEM representations of V_2O_5, (d) V_2O_5 TEM, (e) V_2O_5 EDS, (f) XRD patterns of V_2C and V_2O_5. Reissued from Ref. [140] copyright (2021), with permission from Elsevier.

utilized calcination at high temperatures to produce exceptional one-dimensional nano cuboid V_2O_5 from MXene-V_2C, as illustrated in Fig. 9. Likewise, because of its uniform nano cuboid morphology and configuration steadiness, which support the rapid passage/-diffusion of electrons and Na^+ ionic species while discharge/charge procedure and this matter offered a decent salt elimination functioning of 55.2 mg/g. Besides, a SEM image of V_2C displayed that MXene had a layered structure (see Fig. 10a). While Fig. 10 (b and c) illustrates the complete conversion of V_2C into the one-dimensional ordered nano cuboid after heat treatment, with the extent of every cuboid being 2 μm (Fig. 10 (c and d)). The elemental analysis which displays atomic ratio close to standard ratio, believing that minor fragment of V_2AlC was not altered in material V_2C Fig. 10e, and XRD patterns of V_2C and V_2O_5 proved the successful synthesis of V_2C (Fig. 10f).

4.3. MXene/nanosheets electrodes

In an aqueous medium, MXenes are well recognized for including structural water into their films [141], and the improved ion intercalation kinetics [142] recognized were reliable with reduced charge transfer activation energy at the plane and fast "surface--like'' dispersion inside the interlayer gaps as examined in a figure of 2D substances with nanoconfined liquids [143]. Karthikeyan et al. [144] experimented on 2D MXene materials and applied for the electro-sorption of phosphate and nitrate ionic species from water. The removal of phosphate and nitrate was well defined through a diversity of interactions, containing electrostatic relations, and complication was essential in explaining the adsorption process. The prepared material had a removal efficiency of 89.39 % [145–148].

Amiri et al. [149] recommended and demonstrated the fabrication of exceedingly permeable nitrogen-doped MXene films (N–$Ti_3C_2T_x$) with marvelous potential for saline water purification. The manufacture of N–$Ti_3C_2T_x$ MXene sheets is presented in detail in Fig. 11. Mixing Ti_3AlC_2 substance with concentrated HF solution produced etched $Ti_3C_2T_x$ MXene sheets and N–$Ti_3C_2T_x$ MXene layers were created afterward thermal annealing at 600 °C and followed by washing. Another important lead of the MXene-based CDI material is its extraordinary electro absorption rate. To associate the CDI operation of *N*-doped MXene with recognized substances, an Ashby plot (Fig. 12) is generated. *N*-doped MXene is the individual substance which remains above the recommendation (material index line), offering superior general act with average SAC of 117 ± 4.7 mg/cm^3 (43.5 ± 1.7 mg/g).

Anwer et al. [150] produced 3D nanostructures (CLF@$Ti_3C_2T_x$) via 2D MXene nanosheets (NSs) coated cellulose fibers (CLF). The etching of MAX (Ti_3AlC_2) with HCl mixture in the existence of LiF was employed to eliminate Al contents, as depicted in Fig. 13a–e. Washing and sonication treatment completed the exfoliation. To reinforce the $Ti_3C_2T_x$ NSs and CLF interfacial interaction, as synthesized CLF@$Ti_3C_2T_x$ was thermal-treated in the N_2 environment.

Furthermore, comprehensive TEM inspection was employed to study the shape, crystallinity, and elemental content of distinct CLF, $Ti_3C_2T_x$ NSs, and their nanostructures compound at the nanoscale. CLFs are around 2–3 μm width and tens of μlong, according to the BF-TEM image in Fig. 14a. Besides, CLF has a carbonaceous morphology, as seen in HR-TEM study in Fig. 14b. The resultant planned Fast-Fourier transform (FFT), given as an inset in Fig. 14b, shows a formless kind of CLF. Likewise, produced $Ti_3C_2T_x$ NSs samples were studied, and a BF-TEM appearance of its distinctive unitary film is displayed in Fig. 14c. As demonstrated in Fig. 14d, HR-TEM analysis also let researchers to evaluate the inter-layer gap amongst $Ti_3C_2T_x$ layers (1.2 nm). The existence of extremely well-ordered lattice

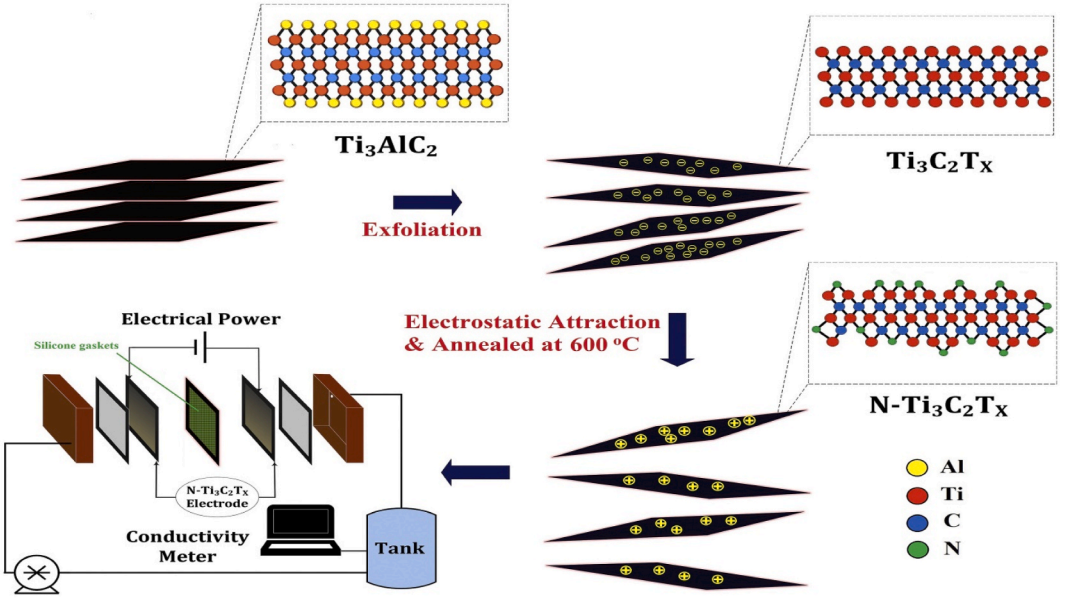

Fig. 11. Manufacture design of the N–$Ti_3C_2T_x$ MXene layers and its use for assembling CDI electrodes. Reproduced from Ref. [149] copyright (2020), with permission from Elsevier.

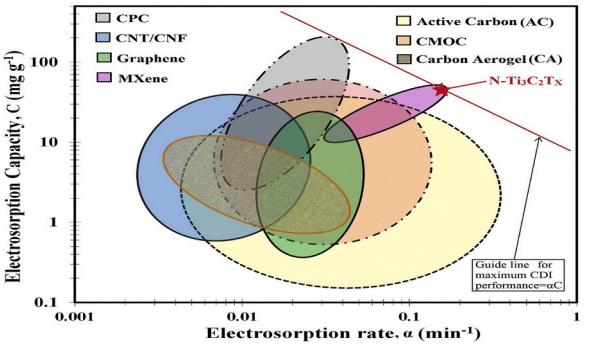

Fig. 12. Ashby plot of electro-sorption capacity vs electro-sorption speed for diverse kinds of materials in literature. Republished from Ref. [149] copyright (2020), with permission from Elsevier.

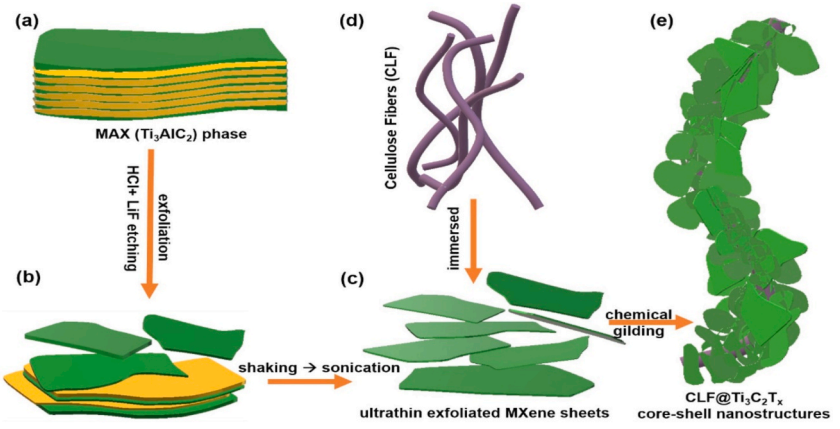

Fig. 13. Diagram demonstration of the synthesis of CLF@$Ti_3C_2T_x$. Republished from Ref. [150] copyright (2021), with permission from Elsevier.

arrangement in as-prepared $Ti_3C_2T_x$ NSs was verified via the inset HR-TEM image of single $Ti_3C_2T_x$ NSs on the basal surface in Fig. 14d [151]. Likewise, the SAED form (inset Fig. 14d) proved the hexagonal arrangement of $Ti_3C_2T_x$ NSs, which exposed the good excellence crystalline configuration of delaminated $Ti_3C_2T_x$ NSs [43,44]. The CLF@$Ti_3C_2T_x$ composite was investigated in detail through HR-TEM method. A usual BF-TEM picture of CLF@$Ti_3C_2T_x$ nanostructures is displayed in Fig. 15a.

Yet, EELS spectroscopy investigation of the mixture was accomplished to verify the C, Ti, and O indications discovered in the core-loss EELS range before elemental mapping. Thus, an EELS spectrum (an inset in Fig. 15b), approving the occurrence of both *C*–K and Ti-L23 energy deficit edges at 283 and 456 eV, correspondingly, with a minor *O*–K sign [152] and also shows usual low amplification DF-STEM picture (Fig. 15b), while Fig. 15c displays the elemental mapping selected region. To recognize the surface chemical conditions and define the surface functionalities of as created $Ti_3C_2T_x$ NSs, high-resolution XPS was utilized. CLF@$Ti_3C_2T_x$ nanostructures composite attained a SAC amount of 34 mg/g, which is not only decent but also equivalent to those expensive CDI electrodes that are prepared completely of MXene.

5. Miscellaneous MXene/composite electrodes

Additionally, to above MXene-based electrode materials that were revealed, as revealed in Table 2, additional MXene composite matter have been explored. Flow electrode CDI systems (FE-CDI) have just gained consideration owing to their capability to avoid cross fault, and function in uninterrupted rotations ad infinitum. In a FE-CDI method for the elimination and recapture of ammonia from increased wastewater, $Ti_3C_2T_x$-MXenes were added as 1 mg/mL slurry electrodes. The electrode act was measured through administering the FE-CDI arrangement in batch mode with a 500 mg/L NH_4Cl feed solution at a regular voltage (1.2 and −1.2 V). An extraordinary average adsorption capability of 460 mg/g beside with a low power expenditure of 0.45 kW h/kg [153]. Another work was stated on the fabrication of an NTP/M nanohybrid from Ti_3C_2 MXene by a simplistic and effective solvothermal method. NTP/M confirmed excellent salt elimination operation, with a supreme desalination rate of 29.6 mg/g × min and a unique salt removal capability of 128.6 mg/g [154].

Recent studies on the optimization of heterointerfaces in the covalent organic framework (COF) on MXene heterostructures have achieved excessive CDI functioning in salt elimination of oxygenated brine water. The MXene's great conductivity, reversible ion

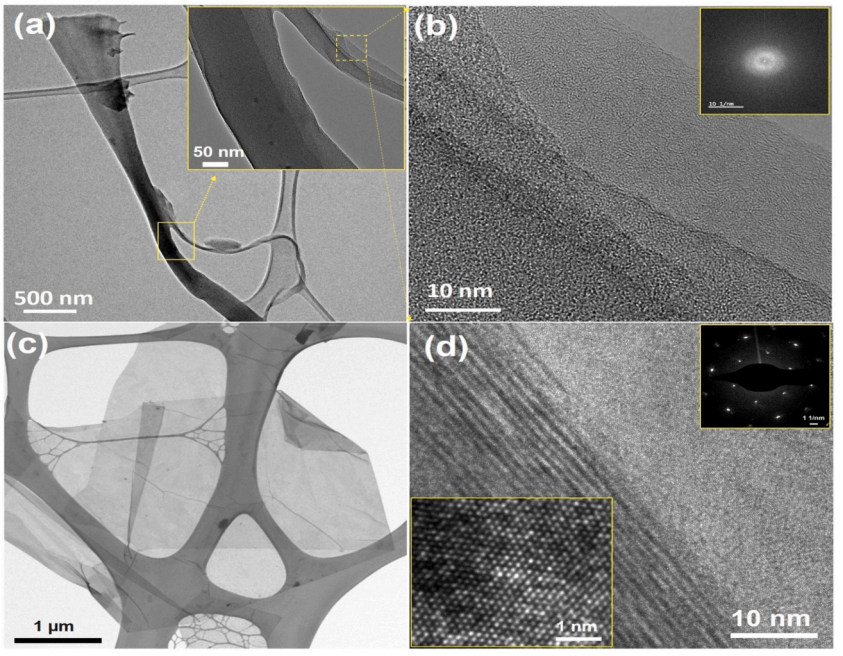

Fig. 14. (A) CLF's BF-TEM figure at low and high magnification (inset); (b) HR-TEM illustration of CLF (inset is the relating FFT pattern); (c) BF-TEM of unitary $Ti_3C_2T_x$ flake; (d) HRTEM picture of vertical cross-sectional $Ti_3C_2T_x$ flake (insets are the HRTEM picture and SAED display of the basal surface of $Ti_3C_2T_x$ NSs. Reproduced from Ref. [150] copyright (2021), with permission from Elsevier.

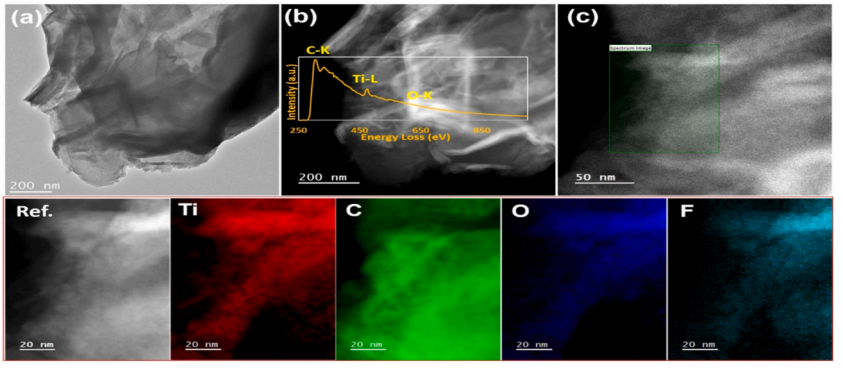

Fig. 15. (A) BF-TEM picture of CLF@$Ti_3C_2T_x$; (b) DF-TEM depiction of CLF@$Ti_3C_2T_x$ (inset is the related EELS spectrum); (c) DF-STEM photo of CLF@$Ti_3C_2T_x$ with rectangular chosen region, and resembling elemental mapping. Republished from Ref. [150] copyright (2021), with permission from Elsevier.

intercalation/deintercalation capability, COF hierarchical porosity, gigantic porosity, and amazing redox are all carried over into the 2D heterostructure with excellent core-shell design. With a greatest adsorption capability of 53.1 mg/g in oxygenated salty water, the MXene@COF heterostructure revealed exceptionally steady cycling operation over the course of 100 CDI cycles and surpassed other MXene-based or 2D materials. This analysis brought consideration to the need for heterointerface optimization in MXene-organic 2D heterostructures to increase CDI of ordinary (oxygenated) saline water [155].

Beside this, Agartan et al. investigated the working of electrodes prepared of $Ti_3C_2T_x$-MXene in a symmetric MCDI approach. $Ti_3C_2T_x$ was prepared via selectively etching the Ti_3AlC_2 MAX phase in a 30 % HF aqueous medium, and the free-standing conductor was composed through applying the paste to a depth of 140 μm. The highest SAC outcome was 8.88 mg/g and the charge efficiency was 74.47 % attained [156].

Jiayi et al. [157] manufactured hydrogel (MNH) composites comprising MXene via a vibrant poly (vinyl alcohol)-based system interrelated via diol-borate ester linking. The material quickly returns its arrangement, physical characteristics, and capacitive functioning afterward restoration, and shifts to a new form in the genuine use environment. The mechanical characteristics of the MNH electrode are excellent, with a self-healing efficiency of 92 % and electrochemical restorative outcomes of 95.8 %. At a current extent of 10 mA/g and a voltage window of 1 V, the electrode had a SAC of roughly 51 mg/g and demonstrated outstanding cycle stability.

Table 2
Desalination functioning of different MXene electrodes in CDI.

Precursor	MXene Electrode material	Synthesis route	Cell architecture	Electrosorption capacity (mg/g)	Surface area (m^2/g)	Primary concentration (mg/L)	Charge efficiency (%)	Applied Voltage (V)	Remarks	Reference
Ti_3ALC_2	Ti_3C_2 MXene	Conventional process	Flow by	13 ± 2	6	292.5	–	1.2	MXene CDI electrodes retained consistent performance for 30 cycles.	[117]
Ti_3ALC_2	Porous N– $Ti_3C_2T_x$	Thermal annealing process	Flow by Symmetric CDI setup	43.5 ± 1.7	368.8	5000	–	1.2	Outstanding electrochemical stability of 99.75 %, and a favorable volumetric capacitance (514 F/cm^3). SAC of 117 4.7 mg/cm^3, with steady performance about 24 CDI cycles.	[149]
$(Mo_{2/3}Sc_{1/3})_2AlC$	$Mo_{1.33}C$-MXene	Acid treatment method	Flow by	5/9/15	1	5/50/600 mM	95	1.4	This MXene successfully completed desalination cycles ranging from low to high salinity concentrations.	[118]
Ti_3ALC_2	$Ti_3C_2T_x$ MXene	LiF/HCl-etching method	Flow by Batch mode method	67.7	2.1	585	–	1.2	Comparatively low power expenditure of 0.24 kW h/kg-NaCl, and the power regaining was 5.44 %.	[159]
Ti_3ALC_2	Preconditioned $Ti_3C_2T_x$ MXene	30 % HF etching	Symmetric MCDI setup + ion exchange membranes	9.19	–	10 mM	73–83	−1.2 (discharge potential (V)	–	[156]
Ti_3ALC_2	Ar plasma-modified $Ti_3C_2T_x$	Wet chemical etching method	Flow by Anode: AC + anionic membrane Cathode: Ti_3C_2 Batch mode	26.8	–	500	–	1.4	The interlayer space for the MXenes $Ti_3C_2T_x$ was improved for proficient Na^+ ionic specie passage via Ar plasma. Salt elimination proficiency and acquired an extreme salt elimination rate of 9.4 mg/g × min.	[134]
Ti_3ALC_2	$Ti_3C_2T_x$ MXene	Minimally intensive layer delamination (MILD) synthesis method	Flow through Anode: MXene Cathode: AC Batch mode	460	–	500 (NH_4Cl)	58–70	1.2	Low energy expenditure of 0.45 kW h/kg with a 92 % restoration efficacy.	[153]
Ti_3ALC_2	NTP/MXene	solvothermal conditions	HCDI Anode: Carbon Cathode: NTP/MXene Batch mode setup	128	–	1000	95	1.8	Maximum desalination rate of 29.6 mg/g × min, with a very high desalination ability and cycling stability over 20 cycles.	[154]
Ti_3ALC_2	Binder-free $Ti_3C_2T_x$ MXene	MILD method	HCDI Carbon electode + anion exchange membrane MXene + cation exchange membrane	39	–	1 M	–	1.2	Volumetric capacitance up to 250 F/cm^3 with a rate retention of 65 %.	[160]
Ti_3ALC_2	$Ti_3C_2T_x$/Ag	oxidation-reduction method	Flow by Batch mode method	135 mg Cl^-/g		10 × 10^{-3} M	95	20 mA/g C. Current	A salt exclusion rate of 1.5 mg/g/min Cl^- at a low power	[158]

(*continued on next page*)

Table 2 (*continued*)

Precursor	MXene Electrode material	Synthesis route	Cell architecture	Electrosorption capacity (mg/g)	Surface area (m^2/g)	Primary concentration (mg/L)	Charge efficiency (%)	Applied Voltage (V)	Remarks	Reference
									usage of 0.42 kW h/kg Cl^- was achieved.	
Ti3AlC2	CLF@ $Ti_3C_2T_x$ nanostructures	conventional gilding process,	symmetric capacitive deionization (CDI) cell	34	–	1 M	–	1.2	In comparison to pure MXene, the CLF@ $Ti_3C_2T_x$-based effective electrodes revealed decent definite capacitance of 142 F/g and extraordinary SAC (35 mg/g).	[150]
Ti_3AlC_2	Asymmetric DSAC//MAX electrodes	dispersed in 10 mL of ammonium hydroxide solution (30 %) via bath sonication	Asymmetric pseudocapacitive cell Anode: DSAC Cathode: MAX (Ti_3AlC_2)	38.6	–	120 ($Cr_{(VI)}$)	–	1.2	Electrochemical redox exchange of $Cr_{(VI)}$ to $Cr_{(III)}$ ionic species. Potential for removal of hazardous contaminants from industrial effluents.	[135]
Ti_3AlC_2	AC//NaOH–$Ti_3C_2T_x$	(NaOH– $Ti_3C_2T_x$) was synthesized by a facile procedure. $Ti_3C_2T_x$ (1 g) was dispersed in 20 mL of 2 M NaOH solution for 6 h	HCDI Anode: AC Cathode: NaOH-MXene	16.02	–	500	82.6	1.2	Asymmetric CDI cell achieved a good electrosorption capacity and a higher charge efficiency compared with the symmetric one comprised of AC. Confirmed stability exceeding 20 cycles.	[130]
Ti_3AlC_2	L-*S*- $Ti_3C_2T_x$	Vacuum-assisted filtration process	HCDI Anode: MXene Cathode: AC	72	–	10 mM	–	1.6	Capacitance (169 F/g at 5 mV/s) and durable cycling constancy (sustained 91.7 % of the primary capacitance after 5000 rounds).	[89]
Ti_3AlC_2	Na^+- $Ti_3C_2T_x$ -MS	Molten-salt synthesis followed by HF-etching	CDI Anode: AC Cathode: Na^+- $Ti_3C_2T_x$	14.8	135	100	81	1.2	Good electrosorption capacity, high charge efficiency and decent cycling stability. Superior desalination performance ascribed to more ion adsorption positions and smaller ions dispersion route owing to subsize of particles.	[126]

Another approach was achieved for $Ti_3C_2T_x$/Ag electrodes that were produced by a casual redox process and later primary utilized as an anode for Cl^- ionic specie gain in electro sorption procedure. All $Ti_3C_2T_x$/Ag materials exhibited small charge transmission hindrance and are hydrophilic. The $Ti_3C_2T_x/Ag^{-3}$ electrode has exceptional desalination amount (135 mg Cl^-/g at 20 mA/g in 0.001 M NaCl solution), steadfast rate ability (1.5 mg Cl^-/g × min at 50 mA/g), decent regeneration, and low power expenditure (0.42 kW h/kg Cl^-). Hence, they proposed a procedure where the salt elimination performing of $Ti_3C_2T_x/Ag^{-3}$ can be attributed to the synergistic consequence among the battery and pseudocapacitive performances (layered-structure $Ti_3C_2T_x$), that may be employed to purpose electrodes with extraordinary distillation capability and rapid speed ability for CDI operations. To take benefit of the Ag/AgCl conversion reaction, MXene works as both an intercalation electrode and an electron conductive association. The production of $Ti_3C_2T_x$/Ag electrodes is facile and straightforward, making them perfect for electrochemical desalination uses [158].

To create permeable $Ti_3C_2T_x$ designs for CDI appliances, $Ti_3C_2T_x$ is exfoliated in chloroform, the suspension that results is frozen in liquid N, and the solid $Ti_3C_2T_x$ cubes are vacuum-dried [119]. Aerogel-like permeable MXene conductor material has a 12 times superior SAC than former carbon-based electrodes, revealed good CDI performance [119]. The porous MXene electrode confirmed exceptional cycling steadiness with an informed SAC of 45 mg/g in a 10,000 mg/L solution (up to 60 cycles). In addition to capacitive storage, chemical species intercalation into the interlayer gap of the MXene influences to salt capture. The electrode's improved working was accredited to the $Ti_3C_2T_x$'s high electrical conductivity, large SA, distinct porous arrangement, and hydrophilicity. Wang et al. [134] improved the SAC of $Ti_3C_2T_x$ to 26.8 mg/g via exposing the interlayer of MXene $Ti_3C_2T_x$ to Ar plasma. The SEM depiction of $Ti_3C_2T_x$ MXene in Fig. 16a exhibits that following the ultrasonic delamination process, multilayer $Ti_3C_2T_x$ develops few-layer or even single-layer $Ti_3C_2T_x$. The results of TEM are presented in Fig. 16b and c. The layered 2D structure of delaminated $Ti_3C_2T_x$ MXene is revealed in Fig. 16b. Fig. 16c displays a few-layer $Ti_3C_2T_x$ with an interlayer gap of 1.28 nm. Vacuum filtration produced a freestanding $Ti_3C_2T_x$ film (Fig. 16d). The as-prepared Ti_3C_2Tx film may be freely folded in Fig. 16e, exhibiting its excellent flexibility. Since a freestanding electrode, $Ti_3C_2T_x$ film prevents the utilization of a binder and conductive agent. Still, when related to slurry coating film electrodes, the freestanding $Ti_3C_2T_x$ film electrode proficiently stops active elements from falling off the collectors. The SEM picture of a cross-section of free-standing $Ti_3C_2T_x$ sheet is presented in Fig. 16f.

The improved interlayer gap between the layers as a consequence of the Ar plasma variation of MXene nanosheets led to advanced salt elimination functioning [134]. Using Ar plasma treatment, the $Ti_3C_2T_x$ surface was altered to pioneer formless carbon and anatase TiO_2 layers. The maximal elimination ability of 26.8 mg/g was attained in 500 mg/L (1.2 V). For numerous cycles of adsorption and desorption, the Ti_3C_2-based electrode proved decent restoration capability and reliable outcomes. In addition, Functioning features like flow speed, half-cycle length (HCL), and discharge potential had an influence on the ionic species elimination working of the MXene material [156].

6. Energy recovery in CDI

6.1. Conventional CDI electrode energy recovery

This is an interesting and quickly growing domain of CDI wherein certain amount of the energy consumed in the deionization practice can be regained. Once the deionization phase is complete, there is chance of reprocessing the energy saved in capacitive units. The renewing utilization of energy in CDI system involves transferring the power stored in the CDI cell once it has reached saturation to new cells that are starting their deionization phase, forming a cycle that produces deionized water. The electrical type and mathematical description of an up/down DC/DC converter are employed to produce this recovered energy. This converter handles the voltage that each of the deionization modules receives. The converter's primary goal is to reduce energy losses through the transfer of power between stages. Propelling slurry in FCDI (Flow capacitive deionization) undoubtedly allows for the possibility of extra energy consumption [161], while energy recovery in CDI has been claimed to be as high as 83 % [162].

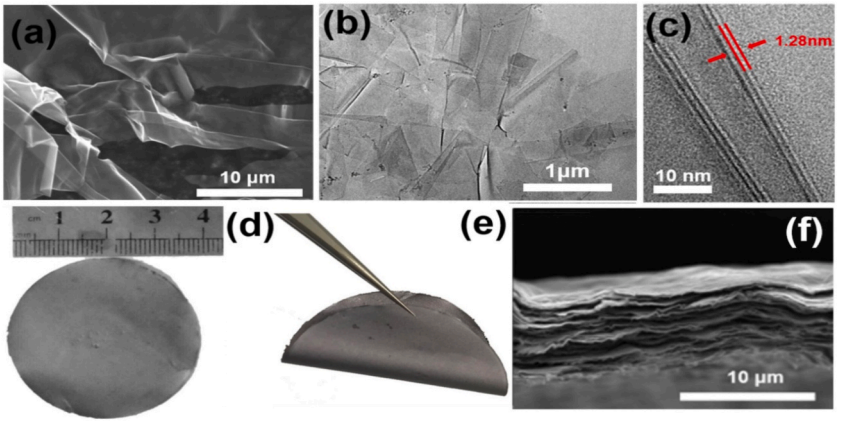

Fig. 16. (A) SEM depiction of $Ti_3C_2T_x$ after ultrasonic delamination; (b), (c) TEM photo of $Ti_3C_2T_x$; (d), (e) free-standing $Ti_3C_2T_x$ layer; (f) SEM representation of cross section of free-standing $Ti_3C_2T_x$ sheet. Reissued from Ref. [134] copyright (2018), with permission from Elsevier.

6.2. Faradaic electrode material energy recovery

In recent times, several faradaic substances have been widely investigated for water salt removal, inspired via energy storage devices. Intercalation or redox practices, which keep chemical entities in the majority of the electrode instead of capacitively on the external. As a result, they appear to have a better capability to remove salt ions than traditional carbon composites [163]. Sodium manganese oxide, a layered designed substance, has been intensively investigated in sodium ion battery (SIB) owing to their extreme capability and low expense. In 2012, innovative research on the use of faradaic electrodes in water distillation was published [164]. They presented a desalination battery with a positive electrode made of $Na_{2-x}Mn_5O_{10}$ nanorods and a negative electrode made of Ag/AgCl. Yet, this method was primarily used as a power load device, with merely a few hundreds of microliters of saline water being removed at a static rate. A hybrid CDI approach was recently created through integrating a battery ($Na_4Mn_9O_{18}$) with a CDI electrode probe (AC), displaying enhanced desalination capability of 31.2 mg/g over a typical carbon-based CDI system [165]. Battery electrode-based CDI, on the other hand, can attain better desalination ability and is similarly suited for salty water with high concentrations due to a different sodium capture mechanism than carbon-based materials. Thus, another significant benefit of employing a CDI battery electrode is that the co-ion consequences of the carbon electrode may be avoided. As a result, IEM-free CDI can be accomplished, making it extra condensed and allowing for small structure. It is important to remark that composite matters might be taken into account in forthcoming study. According to SIB research, appropriate composite materials can increase ion and electron transport efficiency [32,163]. This approach could be utilized to improve CDI's salt elimination performing. Some composite electrodes, in particular, may be able to combine the faradaic and EDL adsorption rules to improve salt removal [35]. Furthermore, it is probable to employ the notion of combined and/or self sustained electrode in SIBs to the electrode plan of CDI, which will simplify the system and make large-scale electrode manufacture achievable.

MXene has diverse advantages over other typical 2D materials, for instance graphene, in terms of numerous functional groups and customizable characteristics due to its diverse chemical composition and programmable interlayer space [166]. MXenes have been seen capable for effective Na^+ storage, particularly in SIBs and capacitors, with definite capacities ranging from 30 to 76.2 mA h/g [167]. MXene has the ensuing reasonable benefits as a CDI electrode. Firstly, MXene has a high volumetric capacitance, allowing for excellent SAC. Second, MXene is available to ions other than Na^+, allowing it to be used in real-world feed water applications [168, 169]. MXene also has the usual trait of powerful attraction between sheets like a normal 2D layered material. As a result, it may be utilized as a binder-free conductor, which is useful for small and handy CDI strategies. Nonetheless, the majority of MXene etching techniques use hazardous HF, limiting large-scale MXene synthesis in CDI. The etching procedure will need to be improved in the future to meet the needs of commercial applications.

Recently, it was shown that adding heteroatom dopants to MXene can increase conductance while also lowering the likelihood of restacking [149]. Mingxing et al. [158] used a simple oxidation reduction technique to make $Ti_3C_2T_x$/Ag electrodes, which were subsequently employed as an anode for Cl^- ion capture in electrochemical process. All $Ti_3C_2T_x$/Ag tests showed a low charge transfer resistance and are hydrophilic. Swift rate proficiency (1.5 mg Cl/g × min at 50 mA/g), excellent salt elimination capability (135 mg Cl^-/g at 20 mA/g in 0.001 M NaCl solution), decent cyclability, and low power utilization (0.42 kW h/kg Cl^-) were all features of the $Ti_3C_2T_x$/Ag-3 electrode Therefore, we propose that the desalination efficiency of $Ti_3C_2T_x/Ag^{-3}$ may be attributed to a synergistic interface between the battery and pseudocapacitive performances, which can be operated to devise electrodes with excessive SAC and swift rate proficiency for CDI functions. In order to take benefit of the Ag/AgCl conversion reaction, MXene accomplishes a double function as an intercalation material and an easy, electron passage system. The fabrication of $Ti_3C_2T_x$/Ag electrodes is simple and straightforward, making them ideal for electrochemical desalination applications.

7. Factors affecting MXene-based CDI electrodes performance

In order to acquire an applicable electrosorption procedure, it is crucial to distinguish and know the consequence of the principal factors changing the electrochemical separation method. This allows us to enhance the strategy as well as the functioning circumstances in order to achieve a specific efficacy goal.

7.1. Effects of parameters on MXene

7.1.1. Effect of etching/delamination on MXene

The investigating unit at Drexel University identified the first MXenes in 2011 via wet chemically etching Al out of the MAX phase Ti_3AlC_2 [170]. The etching technique caused in multilayered MXenes having accordion-like structure when Ti_3AlC_2 powder was added to a 50%wt hydrofluoric (HF) acid solution at ambient temperature [170]. Furthermore to producing a single form of promising 2D matter, this work on exfoliating the MAX stage into 2D nano-crystal MXenes has similarly recommended the opportunity of creating new MXenes from several MAX stages, potentially introducing the access for the progress of a number of 2D materials with connected structures in the future [170]. The MXene made via the HCl/LiF mixture etching approach had a greater interlayer gaps of 1.28 nm (1 nm for HF-etching), as well as an increase in –O and less –F functionalities on the material, which boosted the material's hydrophilic nature. The increased mobility of water particles as a result aids the movement of Na^+ and Cl^- ions between $Ti_3C_2T_x$ layers. The average SAC of the HCl/LiF-etching MXene was 68 mg/g, which was between the maximum in free standing MXene alone electrodes. Furthermore, multilayered MXene is additional delaminated to yield separate or few layered materials through initial inserting organic particles and then sonication. The delamination technique revealed to improve the surface area of MXene, hence increasing its power storage capability and electrosorption quantity [171]. The re-stack concern of delaminated MXene, like that of other 2D materials, has

always been a hindrance to its operation when manufactured into conductors. To address this drawback, the vacuum freeze-drying practice halted the re-stacking of the delaminated MXene nanoflakes. The generated permeable $Ti_3C_2T_x$ MXene conductors attained a great SAC of 118 mg/cm^3 or 45 mg/g (10,000 mg/L salinity at 1.2 V) steady capable of 60 rounds, related to the MXene material with restacked films. In addition, the *N*-doping technique has prevented MXene flakes from restacking, increased electrochemical stability by delaying MXene electrode oxidation, and formed a spongy structured association. The desalination implementation of built *N*–$Ti_3C_2T_x$ MXene electrodes CDI unit produced an average SAC of 43.5 ± 1.7 mg/g (5000 mg/L saline water) around 24 rounds and demonstrated strong capacitance with high surface area 514 F/g and 368.8 m^2/g, respectively [149].

7.1.2. Effect of intercalant on MXene electrode

As previously mentioned, stacked MXene films normally necessitate intercalation to enlarge the interlayer gap and can thus be delaminated into distinct 2D MXene scales [59,114,121]. Several chemical compounds, including DMSO and tetrabutylammonium hydroxides (TBAOH), have been used as intercalants to deteriorate the interlayer connections between MXene layers and aid delamination. The size of the generated MXene fragments can be changed via sonication followed by intercalation [59]. The flake diameters of $Ti_3C_2T_x$ MXene are typically some hundred nanometers after sonication when big organic molecules like DMSO are intercalated [114], as extensive discussion is given in the preceding section. When using TBAOH, however, handshaking is sufficient to produce a suspension of delaminated MXene (V_2CT_x) chips with a size of some micrometers [121]. Picking the right intercalation procedure will alter not only the size of the ensuing MXene flake [59], but likewise their characteristics, impacting the target application's performance. According to Feng et al. [172], the electrode formed from NH_4HF_2 etched MXene underwent intercalation of $NH4^+$ ionic species, which resulted in enhanced interlayer distance and improved hydrophilicity, allowing the created electrode to have a higher capacitance of up to 78 F/g and a desalination capability of 12.1 mg/g. Furthermore, the NH_4HF_2-etched Ti_3C_2 electrode's regeneration ability was determined to be good.

7.1.3. Effect of surface functionalities on MXene electrode

Various functional groups, for instance –F, –OH, and –O, are frequently applied to the surface of manufactured MXenes. Surface functionalities will alter depending on the etchant. According to a study, in case of HF etching produces a 4 times more –F terminations than LiF and HCl solution, whereas the second often produces –O functionalities [173]. Various investigations have shown that the MXene's plane terminations can greatly impact its characteristics in several ways, comprising hydrophilic nature, electrical, and magnetic features, mechanical properties, and even optical aspects. MXene's surface terminations perform a crucial part in the material's electrical characteristics. Improving CDI performance via altering the surface functional groups of MXene is a viable option. When a particular cell voltage is employed, the surface functionality provides a negative standing charge of MXene, which causes the potential sharing to be imbalanced. When performing an electrochemical measurement on the unit with similar MXene electrodes, Srimuk et al. [117] discovered that the capacity of the MXene electrode pair changed 250 mV poorly in contrast to Ag/AgCl when related to the AC electrode pair. They also discovered that, unlike AC electrodes, which have a single symmetric potential dispersal, the MXene electrode set had an imbalanced potential distribution with +0.4 V and −0.6 V at an anode and cathode correspondingly versus Ag/AgCl (1.0 V cell voltage), resulting in good capacitance up to 132 F/g. Guo et al. [134] employed Argon plasma practice to rebuild the surface terminations of Ti_3C_2Tx MXene via eliminating the –F and substituting them with –OH/ = O functionalities, resulting in increased hydrophilic character. The Argon plasma method likewise raised the interlayer space of MXene to 12.6 from 9.7 in basic HF-etched MXene, allowing ions in the electrolyte to diffuse more quickly. When compared to NaOH-treated MXene, the modified MXene had a significantly higher specific capacitance. At 1.2 V, the system produced an excessive SAR of 9.4 mg/g × min and a general improved SAC of 26.8 mg/g when the Ar plasma changed MXene conductor was combined with an AC electrode in an HCDI unit.

7.1.4. Effect of salinity on MXene electrode

Agartan et al. [156] experimented the outcome of distinct operational variables on the distillation working of MCDI utilizing same MXene electrodes, comprising discharge power, HCL, and flow speed. They discovered that a lower discharge potential increases both SAC and SAR, while a longer HCL increases SAC but decreases SAR. Furthermore, swifter flow speeds reduced mutually by 20 %. Torkamanzadeh et al. [133] used electrode load balancing and system voltage regulation to improve the salt elimination working with MXene/CNT electrode (HCDI) combined alongside an AC electrode in brackish water and sea water.

It has been demonstrated to have a steady desalination functioning around 100 rounds, with a SAC of able to 12 mg/g and charge efficiencies of over 80 %. Permselectivity is an extent of a membrane's capability to distinguish between anionic and cationic species, and MXene electrodes have this property as well: only Na^+ ions can be intercalated between the flakes because Cl^- ions are prohibited by MXene's negatively charged surface terminals. As a result of this phenomenon, the counter electrode, (AC), was forced to electro-absorb the Cl^- ions, creating it permselective. Unevenly distributed electrode potential can also aid this permselective tendency. By avoiding the discharging of AC electrode in the 0 V range, the permselectivity will most possible be preserved, limiting the co-ion impact, and ensuing in an extraordinary charge efficiency of approximately 100 % for a 600 mM NaCl solution.

7.2. Energy consumption study of MXene and current desalination techniques

One of the most significant challenges in desalination is energy usage. In the current global energy crisis, it does not seem appropriate to discuss desalination performance without taking energy usage into account. Specific energy consumption (SEC) is a term that is frequently employed to describe the power budget of a salt elimination method. The SEC is measured in kWh/m^3 and is the amount of energy required to create one cubic meter of filter at a given water recovery [174]. There has been numerous desalination

techniques examined so far, the detailed discussion is given the previous article [9]. Table 3 displays the energy expenditure, cost efficiency and mechanism. The total electrical power utilized in electrochemical practices related to one cubic meter formed is how SEC is stated in those processes.

$$SEC = \frac{W_{CDI}}{V_{perm.}} = \frac{\int P_{(t).dt}}{V_{perm.}} \quad (4)$$

Here W_{CDI} is the energy provided, Ᵽ is the applied power, t (time of treatment), and V_{perm}. Is the volume of desalted water. Equation (4) can then be given as below:

$$SEC = \frac{U.\int I(dt).dt}{V_{perm.}} \quad (5)$$

Here U is the electrical potential, t (treatment time), and I(t) is the definite applied current (amperes) at a specific moment. Though, as CDI (as well as ED) focus on or aim the solute rather than the solvent, it appears more suitable to quantify energy expenditure in terms of kWh/kg of salt eliminated rather than kWh/m^3. Until recently, MXene electrode materials have been the subject of extensive investigation. Mohammad et al. [133] studied the electrochemical process of low and high NaCl strengths in aqueous environments via the dissimilar hybrid CDI employing MXene-CNT paired with AC. They focused on the mechanical element of the desalination process rather than optimizing for the highest-possible desalination parameters. Comparing MXene-CNT CDI probes before and after more than 100 rounds of process, understandings into running steadiness and degradation procedures were acquired. Mingxing et al. [158] investigated that $Ti_3C_2T_x$/Ag electrode exhibited outstanding salt removal operation with a capability of 135 mg/Cl^- g at 20 mA/g (0.001 M NaCl solution). Additionally, a salt elimination rate of 1.5 mg/Cl^- g min at 50 mA/g was reached, with low power utilization of 0.42 kW h/kg Cl^-. Hence, research proposes that the synergistic influence between the battery and pseudocapacitive performances can be attributed to the desalination working of $Ti_3C_2T_x/Ag^{-3}$. When creating electrodes for CDI uses, this outcome can be leveraged to produce electrodes with an excessive purification ability and rapid rate proficiency. A novel one-dimensional nano cuboid V_2O_5 was created by Liu et al. [140] from MXene-V_2C, and it revealed good desalination capacity (55.2 mg/g) thanks to its regular nano cuboid organization and structural constancy, which allowed for quick electron and Na^+ ion migration and diffusion during the discharge and charge process. When the procedure was effective, a remarkably low power usage of 0.27 kW h/kg NaCl was attained.

8. Long-term stability of MXene-based CDI electrodes

An essential aspect from the technical opinion of any technology (like desalination technologies) relies on the long-term performance. CDI electrodes have a long operational lifetime since they do not directly engage chemical processes [134]. Investigations utilizing carbon-based CDI electrodes, on the other hand, revealed degradation for instance anode oxidation, which interfered with charge transfer [179–181], In CDI systems, the electrode point of zero charge can be changed, and salt elimination can be diminished [179,182]. Consequently, traditional CDI electrodes may only endure a few hundred charge/discharge cycles, with significant degradation visible within 50 cycles [183,184]. MXene electrodes for CDI, on the other hand, have exhibited amazing stability. Ma et al. [159] found a 10 % improvement in salt adsorption capacity after 50 CDI rounds, which they attributed to sodium intercalation within the interlayer distance, which increased water and ion mobility.

Similarly, after 5000 cycles with a $Ti_3C_2T_x$ electrode, a 3 % rise in initial capacitance was recorded [185]. Shen et al. [89] found that 92 % of primary capacitance was retained after 5000 rounds, whereas Amiri et al. [149] found that 99.8 % of initial conductance was retained after 2000 cycles. Srimuk et al. [117] detected morphological changes as well as steady desalination operation after 40 rounds. Despite the fact that the electrodes displayed higher “exfoliation” during polarization owing to frequent ion intercalation/deintercalation and anode oxidation, the MXene structure was said to have preserved overall integrity.

Lipatov et al. [186] created a form of suitable $Ti_3C_2T_x$ flakes that are practically steady and greatly conductive even after 70 h in the air. Shuck et al. [187] proposed that a key feature in the thermodynamic stabilization of MXene manufactured via the LiF + HCl etching manner was the surface terminations and cations that were chemisorbed on the exterior and inserted in the interlayers. As a result, MXene electrode stability in CDI designs was dependent on the ion intercalation procedure, which is highly influenced via

Table 3
Energy expenditure of MXene-CDI to other conventional desalination systems [9].

Desalination system	Mechanism	Energy expenditure (kWh/m^3)	Water expense (US$/$m^3$)	Reference
Brackish Water Reverse Osmosis (BWRO)	Pressure driven	1.5–2.5	0.26–12	[175]
Sea Water Reverse Osmosis (SWRO)	Pressure driven	4.0–6.0	0.45–1.71	[175]
Multistage Flash Distillation (MSF)	Thermally driven	2.5–5.0	0.56–1.75	[176]
Multiple Effect Distillation (MED)	Thermally driven	2.5–5.0	0.52–8.0	[177]
Liquid-Liquid Extraction (LLE)	Chemically driven	6.0	0.40	[177]
Forward osmosis (FO)	Concentration driven	3–8	0.80	[178]
Electrodialysis (ED)	Potential driven	0.7–5.5	0.6–1.-5	[175]
Capacitive deionization (CDI)	Potential driven	0.594	0.11	[177]
$Ti_3C_2T_x$/Ag (HCDI)	Potential driven	0.42 kW h/kg	–	[158]
V_2O_5/MXene (HCDI)	Potential driven	0.27 kW h/kg	–	[140]

MXene interlayer distance changing over time. The frequent cycles of ions intercalation/deintercalation might produce volume changes in the electrode that has been utilized for a long time, resulting in capacity fading [188,189]. Cycle stability is also critical for extending the life of the MXene electrodes in CDI. Srimuk et al. [118] observed that after 100 charge/discharge cycles, the process was constant and retained 90 % of the preliminary specific capacitance. Though there are some long-term investigations on MXene electrode running, these consequences suggest that CDI electrodes made from MXenes may have higher lifetime and better long-term performance.

Given above, Table 4 reviews certain of the as-explained MXene and MXene based CDI electrodes and their obtained results.

9. Conclusion, perspectives, research gaps and prospects

MXenes and its composites have displayed incredible benefits, and they have developed as perfect applicants for upcoming desalination technology. In spite of copious difficulties that must be addressed, based on the favorable outcomes from the present investigation, an extraordinary progress in the production procedures and uses of these distinctive nanomaterials is predictable in the near future. Different methods were developed in order to examine the deformation and failure in MXene-derived substances. Further, combination of in situ mapping techniques have been investigated.

Additionally, many MXene and MXene-composites electrodes have acquired exceptional electrosorption capability comparing to other carbon allotropes (Table 3). Besides, MXene electrodes (symmetric architecture) have shown excellent SAC value except to some MXene-composites i.e., NTP/MXene, $Ti_3C_2T_x$/Ag. While other composites yielded high stability with good electro sorption performance (Table 1). However, in order to acquire an efficient SAC, selecting etchant is important to increase the interlayer space as well as an increase the oxygenated functionalities. Also, the delamination procedure shown to enhance surface area of MXene, hence increasing its charge storage capability.

This review revealed several concerns that should be studied and must be incoprporated while reporting reaserch papers in this field of CDI for the purpose of uniformity, inclusivity and comparability

1. The electrochemical performance of an electrode should be evaluated in CDI under circumstances that are as close to reality as feasible, with the factors, for instance system formation, electrolyte strength, power window, and electrode status (stationary or related), corresponding to the proper values. This will establish a trustworthy correlation between an electrode's capacitance and salt removal capacity.
2. Researchers are strongly encouraged to reveal the performance matrices. In particular, the SAC quantities and ions elimination speeds of the electrodes can both be concurrently discovered using the CDI Ragone plot or the Kim-Yoon plot. These investigations act as databases, allowing an association of diverse CDI electrodes with numerous salt removal methods in the upcoming time (as, EDLC, pseudo capacitance, and charged species intercalation power storage).
3. It is probable that the use of these innovative materials for CDI will spread as a result of the advancements made in the progress of SCs, LIBs, and SIBs. However, in order to gain an accurate assessment of a CDI unit's desalination performance, tests should not be performed on a CDI design with minute electrodes (e.g., weighing a few micrograms), which are more appropriate for actual uses in CDI.
4. MXenes are still prepared in lab scale quantity, thus there is a need of ecofriendly and cost-efficient synthesis protocols for large scale applications.
5. Leaching issues related to MXene derived CDI electrodes should be evaluated in each paper.
6. Harmful effect of MXene on ecosystem, if directly released in the environment should be estimated.
7. Elements of economic analysis should be provided for every new development. Energy expenditure seems to be a one of useful parameters making possible the comparison of costs between different attempts.
8. It is recommended that every research work should include the study of energy consumption of materials in order to understand it effectively.

Furthermore, it can be foreseen according to the current data, that.

1. MXene electrodes could offer even superior SAC if the full aptitude of the material's redox and intercalation characteristics could be comprehended.
2. Pseudocapacitor ion storage may be more likely to be advanced, and it characteristically has a better SAC value than EDLCs adsorption.
3. Additionally, more research should be done on the MXene system architecture and salt adsorption rate (SAR), which is frequently disregarded in MXene investigations. To attain enhanced SAR, there should be highly reversible ion intercalation/deintercalation throughout the charging and discharging procedure, as well as superior electrical conductivity and excellent mechanical strength.
4. MXenes low scalability and high synthesis cost stay to be a barrier to the mass manufacture of the electrodes, which inhibits CDI systems from scaling up. The SAC constancy over numerous cycles is also an interest to move into the next stage of technology readiness, which is presently still at a prototypes stage.

For MXenes to be a forerunner in salt removal, more investigation is crucial to restrain the current difficulties. There is no doubt that MXenes have secured an epoch of the coming generation 2D nanomaterials and will have a brilliant future in water distillation and environmental remediation.

Table 4
MXene and MXene/composites electrode performance summery.

S. No	Electrode material		Energy expenditure (kWh/kg)	SAC (mg/g)	Architecture design	Initial concentration (mg/L)	Applied potential (V)	Synthesis route	No. Of cycles confirming stability	Reference
1	Cathode NaOH–Ti3C2Tx	Anode Activated carbon	NA	16.02	Asymmetric CDI	500	1.2	HF etching	20	[130]
2	MAX (Ti3AlC2)	DSAC	NA	38.6	Asymmetric CDI	120 ($Cr_{(VI)}$)	1.2	Commercially available	10	[135]
3	Ti3C2Tx	Ti3C2Tx	0.24	67.7	Symmetric CDI	585	1.2	LiF + HCl	50	[159]
4	MXene-V2C	Activated carbon	0.27	55.2	HCDI	500	1.2	HF etching followed by calcination	20	[140]
5	N–Ti3C2Tx	N–Ti3C2Tx	NA	43.5 ± 1.7	Symmetric CDI	5000	1.2	Thermal annealing	24	[149]
6	CLF@Ti3C2Tx	CLF@Ti3C2Tx	NA	35	Symmetric CDI	600	1.2	dip-coating method	–	[150]
7	NTP/MXene	Activated carbon	NA	128.6	HCDI	1000	1.8	Solvothermal synthesis	20	[154]
8	Ti3C2Tx/Ag	Ti3C2Tx	0.42	135 mg Cl^-/g	Asymmetric CDI	0.001 M NaCl	1.2	Oxidation-reduction process	–	[158]

Declaration of competing interest

The authors declare that they have no known competing financial interests or personal relationships that could have appeared to influence the work reported in this paper.

Data availability

No data was used for the research described in the article.

References

[1] H. Younes, F. Ravaux, N. El Hadri, L. Zou, Nanostructuring of pseudocapacitive MnFe2O4/Porous rGO electrodes in capacitive deionization, Electrochim. Acta 306 (2019) 1–8.
[2] Y. Zhao, B. Liang, X. Wei, K. Li, C. Lv, Y. Zhao, A core–shell heterostructured CuFe@NiFe Prussian blue analogue as a novel electrode material for high-capacity and stable capacitive deionization, J. Mater. Chem. A 7 (2019) 10464–10474.
[3] L. Guo, Y. Huang, M. Ding, Z.Y. Leong, S. Vafakhah, H.Y. Yang, A high performance electrochemical deionization method to desalinate brackish water with an FePO4/RGO nanocomposite, J. Mater. Chem. A 6 (2018) 8901–8908.
[4] Z. Yue, Y. Ma, J. Zhang, H. Li, Pseudo-capacitive behavior induced dual-ion hybrid deionization system based on Ag@rGO||Na1.1V3O7.9@rGO, J. Mater. Chem. A 7 (2019) 16892–16901.
[5] S. Wang, S. Wang, G. Wang, X. Che, D. Li, C. Li, J. Qiu, Ion removal performance and enhanced cyclic stability of SnO2/CNT composite electrode in hybrid capacitive deionization, Mater. Today Commun. 23 (2020), 100904.
[6] T. Kim, C.A. Gorski, B.E. Logan, Low energy desalination using battery electrode deionization, Environ. Sci. Technol. Lett. 4 (2017) 444–449.
[7] M.E. Suss, S. Porada, X. Sun, P.M. Biesheuvel, J. Yoon, V. Presser, Water desalination via capacitive deionization: what is it and what can we expect from it? Energy Environ. Sci. 8 (2015) 2296–2319.
[8] P.S. Goh, A.F. Ismail, Graphene-based nanomaterial: the state-of-the-art material for cutting edge desalination technology, Desalination 356 (2015) 115–128.
[9] B. Samejo, S. Gul, S. Samejo, N.Q. Abro, N. Yenil, N. Memon, 2021, Carbon Based Electrode Materials and their Architectures for Capacitive Deionization 22 (2021) 33.
[10] T. Gao, Y. Du, H. Li, Preparation of nitrogen-doped graphitic porous carbon towards capacitive deionization with high adsorption capacity and rate capability, Separ. Purif. Technol. 211 (2019) 233–241.
[11] C. Zhao, G. Liu, N. Sun, X. Zhang, G. Wang, Y. Zhang, H. Zhang, H. Zhao, Biomass-derived N-doped porous carbon as electrode materials for Zn-air battery powered capacitive deionization, Chem. Eng. J. 334 (2018) 1270–1280.
[12] Y. Li, J. Shen, J. Li, X. Sun, J. Shen, W. Han, L. Wang, A protic salt-derived porous carbon for efficient capacitive deionization: balance between porous structure and chemical composition, Carbon 116 (2017) 21–32.
[13] X. Xu, H. Tan, Z. Wang, C. Wang, L. Pan, Y.V. Kaneti, T. Yang, Y. Yamauchi, Extraordinary capacitive deionization performance of highly-ordered mesoporous carbon nano-polyhedra for brackish water desalination, Environ. Sci.: Nano 6 (2019) 981–989.
[14] X. Xu, A.E. Allah, C. Wang, H. Tan, A.A. Farghali, M.H. Khedr, V. Malgras, T. Yang, Y. Yamauchi, Capacitive deionization using nitrogen-doped mesostructured carbons for highly efficient brackish water desalination, Chem. Eng. J. 362 (2019) 887–896.
[15] Y. Li, J. Qi, J. Li, J. Shen, Y. Liu, X. Sun, J. Shen, W. Han, L. Wang, Nitrogen-doped hollow mesoporous carbon spheres for efficient water desalination by capacitive deionization, ACS Sustain. Chem. Eng. 5 (2017) 6635–6644.
[16] P. Shi, C. Wang, J. Sun, P. Lin, X. Xu, T. Yang, Thermal conversion of polypyrrole nanotubes to nitrogen-doped carbon nanotubes for efficient water desalination using membrane capacitive deionization, Separ. Purif. Technol. 235 (2020), 116196.
[17] Y. Li, Y. Liu, M. Wang, X. Xu, T. Lu, C.Q. Sun, L. Pan, Phosphorus-doped 3D carbon nanofiber aerogels derived from bacterial-cellulose for highly-efficient capacitive deionization, Carbon 130 (2018) 377–383.
[18] G. Wang, Q. Dong, T. Wu, F. Zhan, M. Zhou, J. Qiu, Ultrasound-assisted preparation of electrospun carbon fiber/graphene electrodes for capacitive deionization: importance and unique role of electrical conductivity, Carbon 103 (2016) 311–317.
[19] X. Xu, Y. Liu, M. Wang, C. Zhu, T. Lu, R. Zhao, L. Pan, Hierarchical hybrids with microporous carbon spheres decorated three-dimensional graphene frameworks for capacitive applications in supercapacitor and deionization, Electrochim. Acta 193 (2016) 88–95.
[20] H. Huang, M. Yan, C. Yang, H. He, Q. Jiang, L. Yang, Z. Lu, Z. Sun, X. Xu, Y. Bando, Y. Yamauchi, Graphene nanoarchitectonics: recent advances in graphene-based electrocatalysts for hydrogen evolution reaction, Adv. Mater. 31 (2019), 1903415.
[21] X. Xu, S. Zhang, J. Tang, L. Pan, M. Eguchi, J. Na, Y. Yamauchi, Nitrogen-doped nanostructured carbons: a new material horizon for water desalination by capacitive deionization, Inside Energy 2 (2020), 100043.
[22] P. Zhang, M. He, S. Huo, F. Li, K. Li, Recent progress in metal-based composites toward adsorptive removal of phosphate: mechanisms, behaviors, and prospects, Chem. Eng. J. 446 (2022), 137081.
[23] P. Zhang, F. Li, M. He, S. Huo, X. Zhang, B. Cen, D. Fang, K. Li, H. Wang, In-situ Construction of Abundant Active Centers on Hierarchically Porous Carbon Electrode toward High-Performance Phosphate Electrosorption: Synergistic Effect of Electric Field and Capture Sites, Green Energy & Environment, 2022.
[24] S. Yang, Q. Wang, H. Zhao, D. Liu, Bottom-up synthesis of MOF-derived magnetic Fe-Ce bimetal oxide with ultrahigh phosphate adsorption performance, Chem. Eng. J. 448 (2022), 137627.
[25] R. Chen, T. Sheehan, J.L. Ng, M. Brucks, X. Su, Capacitive deionization and electrosorption for heavy metal removal, Environ. Sci. J. Integr. Environ. Res.: Water Res. & Technol. 6 (2020) 258–282.
[26] P. Zhang, M. He, F. Li, D. Fang, K. Li, H. Wang, Engineering bimetallic capture sites on hierarchically porous carbon electrode for efficient phosphate electrosorption: multiple active centers and excellent electrochemical properties, J. Mater. Chem. A 11 (2023) 579–588.
[27] M. He, P. Zhang, S. Huo, X. Zhang, A. Gong, W. Zhang, K. Li, Remarkable phosphate electrosorption/desorption by bimetallic MOF-derived hierarchically porous carbon electrode: in-situ creation of multiple active centers and boosting electrochemical activities, Chem. Eng. J. 446 (2022), 137396.
[28] O. Barbieri, M. Hahn, A. Herzog, R. Kötz, Capacitance limits of high surface area activated carbons for double layer capacitors, Carbon 43 (2005) 1303–1310.
[29] B. Zhang, A. Boretti, S. Castelletto, Mxene pseudocapacitive electrode material for capacitive deionization, Chem. Eng. J. 435 (2022), 134959.
[30] P. Sivasubramanian, M. Kumar, V.S. Kirankumar, M.S. Samuel, C.-D. Dong, J.-H. Chang, Capacitive deionization and electrosorption techniques with different electrodes for wastewater treatment applications, Desalination 559 (2023), 116652.
[31] S. Vafakhah, Z. Beiramzadeh, M. Saeedikhani, H.Y. Yang, A review on free-standing electrodes for energy-effective desalination: recent advances and perspectives in capacitive deionization, Desalination 493 (2020), 114662.
[32] F. Zhou, T. Gao, M. Luo, H. Li, Heterostructured graphene@Na4Ti9O20 nanotubes for asymmetrical capacitive deionization with ultrahigh desalination capacity, Chem. Eng. J. 343 (2018) 8–15.
[33] W. Shi, P. Nie, G. Zhu, B. Hu, J. Yang, J. Liu, Self-supporting Prussian blue@CNF based battery-capacitor with superhigh adsorption capacity and selectivity for potassium recovery, Chem. Eng. J. 388 (2020), 124162.
[34] F. Chen, Y. Huang, L. Guo, L. Sun, Y. Wang, H.Y. Yang, Dual-ions electrochemical deionization: a desalination generator, Energy Environ. Sci. 10 (2017) 2081–2089.

[35] Z. Yue, T. Gao, H. Li, Robust synthesis of carbon@Na4Ti9O20 core-shell nanotubes for hybrid capacitive deionization with enhanced performance, Desalination 449 (2019) 69–77.
[36] P.M. Biesheuvel, A. van der Wal, Membrane capacitive deionization, J. Membr. Sci. 346 (2010) 256–262.
[37] Y. Liu, K. Wang, X. Xu, K. Eid, A.M. Abdullah, L. Pan, Y. Yamauchi, Recent advances in faradic electrochemical deionization: system architectures versus electrode materials, ACS Nano 15 (2021) 13924–13942.
[38] S. Kim, J. Lee, J.S. Kang, K. Jo, S. Kim, Y.-E. Sung, J. Yoon, Lithium recovery from brine using a λ-MnO2/activated carbon hybrid supercapacitor system, Chemosphere 125 (2015) 50–56.
[39] B.W. Byles, B. Hayes-Oberst, E. Pomerantseva, Ion removal performance, structural/compositional dynamics, and electrochemical stability of layered manganese oxide electrodes in hybrid capacitive deionization, ACS Appl. Mater. Interfaces 10 (2018) 32313–32322.
[40] L. Guo, R. Mo, W. Shi, Y. Huang, Z.Y. Leong, M. Ding, F. Chen, H.Y. Yang, A Prussian blue anode for high performance electrochemical deionization promoted by the faradaic mechanism, Nanoscale 9 (2017) 13305–13312.
[41] Z. Ding, X. Xu, Y. Li, K. Wang, T. Lu, L. Pan, Significantly improved stability of hybrid capacitive deionization using nickel hexacyanoferrate/reduced graphene oxide cathode at low voltage operation, Desalination 468 (2019), 114078.
[42] S. Liang, C. Han, Q. Meng, G. Tian, Nitrogen and sulfur co-doped NaTi2(PO4)3/hole graphene composite as high-performance electrosorption electrodes for hybrid capacitive deionization, J. Mater. Sci. 55 (2020) 6017–6029.
[43] Y. Liu, J. Chen, B. Cui, P. Yin, C. Zhang, in: Design and Preparation of Biomass-Derived Carbon Materials for Supercapacitors: A Review, C, vol. 4, 2018, p. 53.
[44] Z. Guo, Y. Ma, X. Dong, M. Hou, Y. Wang, Y. Xia, Integrating desalination and energy storage using a saltwater-based hybrid sodium-ion supercapacitor, ChemSusChem 11 (2018) 1741–1745.
[45] J. Cao, Y. Wang, L. Wang, F. Yu, J. Ma, Na3V2(PO4)3@C as faradaic electrodes in capacitive deionization for high-performance desalination, Nano Lett. 19 (2019) 823–828.
[46] M. Naguib, M. Kurtoglu, V. Presser, J. Lu, J. Niu, M. Heon, L. Hultman, Y. Gogotsi, M.W. Barsoum, Two-dimensional nanocrystals produced by exfoliation of Ti3AlC2, Adv. Mater. 23 (2011) 4248–4253.
[47] B. Xu, M. Zhu, W. Zhang, X. Zhen, Z. Pei, Q. Xue, C. Zhi, P. Shi, Ultrathin MXene-micropattern-based field-effect transistor for probing neural activity, Adv. Mater. 28 (2016) 3333–3339.
[48] T. Cai, L. Wang, Y. Liu, S. Zhang, W. Dong, H. Chen, X. Yi, J. Yuan, X. Xia, C. Liu, S. Luo, Ag3PO4/Ti3C2 MXene interface materials as a Schottky catalyst with enhanced photocatalytic activities and anti-photocorrosion performance, Appl. Catal. B Environ. 239 (2018) 545–554.
[49] M. Naguib, Y. Gogotsi, Synthesis of two-dimensional materials by selective extraction, Acc. Chem. Res. 48 (2015) 128–135.
[50] Y. Gogotsi, B. Anasori, The rise of MXenes, ACS Nano 13 (2019) 8491–8494.
[51] M. Hu, T. Hu, Z. Li, Y. Yang, R. Cheng, J. Yang, C. Cui, X. Wang, Surface functional groups and interlayer water determine the electrochemical capacitance of Ti3C2Tx MXene, ACS Nano 12 (2018) 3578–3586.
[52] J. Liu, X. Jiang, R. Zhang, Y. Zhang, L. Wu, W. Lu, J. Li, Y. Li, H. Zhang, MXene-enabled electrochemical microfluidic biosensor: applications toward multicomponent continuous monitoring in whole blood, Adv. Funct. Mater. 29 (2019), 1807326.
[53] M. Naguib, V.N. Mochalin, M.W. Barsoum, Y. Gogotsi, 25th anniversary article: MXenes: a new family of two-dimensional materials, Adv. Mater. 26 (2014) 992–1005.
[54] M. Ghidiu, M.R. Lukatskaya, M.-Q. Zhao, Y. Gogotsi, M.W. Barsoum, Conductive two-dimensional titanium carbide 'clay' with high volumetric capacitance, Nature 516 (2014) 78–81.
[55] J. Halim, M.R. Lukatskaya, K.M. Cook, J. Lu, C.R. Smith, L.-Å. Näslund, S.J. May, L. Hultman, Y. Gogotsi, P. Eklund, M.W. Barsoum, Transparent conductive two-dimensional titanium carbide epitaxial thin films, Chem. Mater. 26 (2014) 2374–2381.
[56] N. Hagemann, K. Spokas, H.-P. Schmidt, R. Kägi, M.A. Böhler, T.D. Bucheli, Activated carbon, biochar and charcoal: linkages and synergies across pyrogenic carbon's ABCs, Water 10 (2018) 182.
[57] M.R. Lukatskaya, J. Halim, B. Dyatkin, M. Naguib, Y.S. Buranova, M.W. Barsoum, Y. Gogotsi, Room-temperature carbide-derived carbon synthesis by electrochemical etching of MAX phases, Angew. Chem. 126 (2014) 4977–4980.
[58] C. Xing, S. Chen, X. Liang, Q. Liu, M. Qu, Q. Zou, J. Li, H. Tan, L. Liu, D. Fan, H. Zhang, Two-dimensional MXene (Ti3C2)-integrated cellulose hydrogels: toward smart three-dimensional network nanoplatforms exhibiting light-induced swelling and bimodal photothermal/chemotherapy anticancer activity, ACS Appl. Mater. Interfaces 10 (2018) 27631–27643.
[59] M. Alhabeb, K. Maleski, B. Anasori, P. Lelyukh, L. Clark, S. Sin, Y. Gogotsi, Guidelines for synthesis and processing of two-dimensional titanium carbide (Ti3C2Tx MXene), Chem. Mater. 29 (2017) 7633–7644.
[60] K. Hantanasirisakul, Y. Gogotsi, Electronic and optical properties of 2D transition metal carbides and nitrides (MXenes), Adv. Mater. 30 (2018), 1804779.
[61] M. Naguib, J. Halim, J. Lu, K.M. Cook, L. Hultman, Y. Gogotsi, M.W. Barsoum, New two-dimensional niobium and vanadium carbides as promising materials for Li-ion batteries, J. Am. Chem. Soc. 135 (2013) 15966–15969.
[62] D. Xiong, X. Li, Z. Bai, S. Lu, Recent advances in layered Ti3C2Tx MXene for electrochemical energy storage, Small 14 (2018), 1703419.
[63] P. Srivastava, A. Mishra, H. Mizuseki, K.-R. Lee, A.K. Singh, Mechanistic insight into the chemical exfoliation and functionalization of Ti3C2 MXene, ACS Appl. Mater. Interfaces 8 (2016) 24256–24264.
[64] M. Naguib, O. Mashtalir, J. Carle, V. Presser, J. Lu, L. Hultman, Y. Gogotsi, M.W. Barsoum, Two-dimensional transition metal carbides, ACS Nano 6 (2012) 1322–1331.
[65] Y. Song, Z. Li, K. Guo, T. Shao, Hierarchically ordered mesoporous carbon/graphene composites as supercapacitor electrode materials, Nanoscale 8 (2016) 15671–15680.
[66] L. Shen, X. Zhou, X. Zhang, Y. Zhang, Y. Liu, W. Wang, W. Si, X. Dong, Carbon-intercalated Ti3C2Tx MXene for high-performance electrochemical energy storage, J. Mater. Chem. A 6 (2018) 23513–23520.
[67] L. Yu, L. Hu, B. Anasori, Y.-T. Liu, Q. Zhu, P. Zhang, Y. Gogotsi, B. Xu, MXene-bonded activated carbon as a flexible electrode for high-performance supercapacitors, ACS Energy Lett. 3 (2018) 1597–1603.
[68] X.-T. Gao, Y. Xie, X.-D. Zhu, K.-N. Sun, X.-M. Xie, Y.-T. Liu, J.-Y. Yu, B. Ding, Ultrathin MXene nanosheets decorated with TiO2 quantum dots as an efficient sulfur host toward fast and stable Li–S batteries, Small 14 (2018), 1802443.
[69] M.-Q. Zhao, C.E. Ren, Z. Ling, M.R. Lukatskaya, C. Zhang, K.L. Van Aken, M.W. Barsoum, Y. Gogotsi, Flexible MXene/carbon nanotube composite paper with high volumetric capacitance, Adv. Mater. 27 (2015) 339–345.
[70] W. Shao, M. Tebyetekerwa, I. Marriam, W. Li, Y. Wu, S. Peng, S. Ramakrishna, S. Yang, M. Zhu, Polyester@MXene nanofibers-based yarn electrodes, J. Power Sources 396 (2018) 683–690.
[71] M. Boota, Y. Gogotsi, MXene—conducting polymer asymmetric pseudocapacitors, Adv. Energy Mater. 9 (2019), 1802917.
[72] R. Sun, H.-B. Zhang, J. Liu, X. Xie, R. Yang, Y. Li, S. Hong, Z.-Z. Yu, Highly conductive transition metal carbide/carbonitride(MXene)@polystyrene nanocomposites fabricated by electrostatic assembly for highly efficient electromagnetic interference shielding, Adv. Funct. Mater. 27 (2017), 1702807.
[73] K. Rasool, R.P. Pandey, P.A. Rasheed, S. Buczek, Y. Gogotsi, K.A. Mahmoud, Water treatment and environmental remediation applications of two-dimensional metal carbides (MXenes), Mater. Today 30 (2019) 80–102.
[74] B. Anasori, M.R. Lukatskaya, Y. Gogotsi, 2D metal carbides and nitrides (MXenes) for energy storage, Nat. Rev. Mater. 2 (2017), 16098.
[75] Y.-J. Zhang, J.-H. Lan, L. Wang, Q.-Y. Wu, C.-Z. Wang, T. Bo, Z.-F. Chai, W.-Q. Shi, Adsorption of uranyl species on hydroxylated titanium carbide nanosheet: a first-principles study, J. Hazard Mater. 308 (2016) 402–410.
[76] J. Zhu, E. Ha, G. Zhao, Y. Zhou, D. Huang, G. Yue, L. Hu, N. Sun, Y. Wang, L.Y.S. Lee, C. Xu, K.-Y. Wong, D. Astruc, P. Zhao, Recent advance in MXenes: a promising 2D material for catalysis, sensor and chemical adsorption, Coord. Chem. Rev. 352 (2017) 306–327.
[77] L. Cheng, X. Li, H. Zhang, Q. Xiang, Two-dimensional transition metal MXene-based photocatalysts for solar fuel generation, J. Phys. Chem. Lett. 10 (2019) 3488–3494.

[78] P. Zhang, L. Wang, L.-Y. Yuan, J.-H. Lan, Z.-F. Chai, W.-Q. Shi, Sorption of Eu(III) on MXene-derived titanate structures: the effect of nano-confined space, Chem. Eng. J. 370 (2019) 1200–1209.
[79] Y. Sun, X. Meng, Y. Dall'Agnese, C. Dall'Agnese, S. Duan, Y. Gao, G. Chen, X.-F. Wang, 2D MXenes as Co-catalysts in photocatalysis: synthetic methods, Nano-Micro Lett. 11 (2019) 79.
[80] Z. Guo, J. Zhou, L. Zhu, Z. Sun, MXene: a promising photocatalyst for water splitting, J. Mater. Chem. A 4 (2016) 11446–11452.
[81] C.E. Ren, K.B. Hatzell, M. Alhabeb, Z. Ling, K.A. Mahmoud, Y. Gogotsi, Charge- and size-selective ion sieving through Ti3C2Tx MXene membranes, J. Phys. Chem. Lett. 6 (2015) 4026–4031.
[82] A. Shahzad, K. Rasool, W. Miran, M. Nawaz, J. Jang, K.A. Mahmoud, D.S. Lee, Two-dimensional Ti3C2Tx MXene nanosheets for efficient copper removal from water, ACS Sustain. Chem. Eng. 5 (2017) 11481–11488.
[83] M.A. Iqbal, S.I. Ali, F. Amin, A. Tariq, M.Z. Iqbal, S. Rizwan, La- and Mn-codoped bismuth ferrite/Ti3C2 MXene composites for efficient photocatalytic degradation of Congo red dye, ACS Omega 4 (2019) 8661–8668.
[84] P. Zhang, M. Xiang, H. Liu, C. Yang, S. Deng, Novel two-dimensional magnetic titanium carbide for methylene blue removal over a wide pH range: insight into removal performance and mechanism, ACS Appl. Mater. Interfaces 11 (2019) 24027–24036.
[85] F. Dixit, K. Zimmermann, R. Dutta, N.J. Prakash, B. Barbeau, M. Mohseni, B. Kandasubramanian, Application of MXenes for water treatment and energy-efficient desalination: a review, J. Hazard Mater. 423 (2022), 127050.
[86] F.A. Janjhi, I. Ihsanullah, M. Bilal, R. Castro-Muñoz, G. Boczkaj, F. Gallucci, MXene-based materials for removal of antibiotics and heavy metals from wastewater– a review, Water Resour. Ind. 29 (2023), 100202.
[87] G.M. Torrie, J.P. Valleau, Electrical double layers. 4. Limitations of the Gouy-Chapman theory, J. Phys. Chem. 86 (1982) 3251–3257.
[88] J. Reedijk, Reference Module in Chemistry, Molecular Sciences and Chemical Engineering, Elsevier, 2014.
[89] X. Shen, Y. Xiong, R. Hai, F. Yu, J. Ma, All-MXene-based integrated membrane electrode constructed using Ti3C2Tx as an intercalating agent for high-performance desalination, Environ. Sci. Technol. 54 (2020) 4554–4563.
[90] C. Zhang, D. He, J. Ma, W. Tang, T.D. Waite, Faradaic reactions in capacitive deionization (CDI) - problems and possibilities: a review, Water Res. 128 (2018) 314–330.
[91] J. Elisadiki, C.K. King'ondu, Performance of ion intercalation materials in capacitive deionization/electrochemical deionization: a review, J. Electroanal. Chem. 878 (2020), 114588.
[92] B. Anasori, M.R. Lukatskaya, Y. Gogotsi, 2D metal carbides and nitrides (MXenes) for energy storage, Nat. Rev. Mater. 2 (2017), 16098.
[93] K.S. Novoselov, A.K. Geim, S.V. Morozov, D. Jiang, Y. Zhang, S.V. Dubonos, I.V. Grigorieva, A.A. Firsov, Electric field effect in atomically thin carbon films, Science 306 (2004) 666.
[94] S. Zhang, T. Ma, A. Erdemir, Q. Li, Tribology of two-dimensional materials: from mechanisms to modulating strategies, Mater. Today 26 (2019) 67–86.
[95] K. Zhu, Y. Jin, F. Du, S. Gao, Z. Gao, X. Meng, G. Chen, Y. Wei, Y. Gao, Synthesis of Ti2CTx MXene as electrode materials for symmetric supercapacitor with capable volumetric capacitance, J. Energy Chem. 31 (2019) 11–18.
[96] A. VahidMohammadi, A. Hadjikhani, S. Shahbazmohamadi, M. Beidaghi, Two-dimensional vanadium carbide (MXene) as a high-capacity cathode material for rechargeable aluminum batteries, ACS Nano 11 (2017) 11135–11144.
[97] B. Soundiraraju, B.K. George, Two-dimensional titanium nitride (Ti2N) MXene: synthesis, characterization, and potential application as surface-enhanced Raman scattering substrate, ACS Nano 11 (2017) 8892–8900.
[98] Q. Tao, M. Dahlqvist, J. Lu, S. Kota, R. Meshkian, J. Halim, J. Palisaitis, L. Hultman, M.W. Barsoum, P.O.Å. Persson, J. Rosen, Two-dimensional Mo1.33C MXene with divacancy ordering prepared from parent 3D laminate with in-plane chemical ordering, Nat. Commun. 8 (2017), 14949.
[99] J. Halim, J. Palisaitis, J. Lu, J. Thörnberg, E.J. Moon, M. Precner, P. Eklund, P.O.Å. Persson, M.W. Barsoum, J. Rosen, Synthesis of two-dimensional Nb1.33C (MXene) with randomly distributed vacancies by etching of the quaternary solid solution (Nb2/3Sc1/3)2AlC MAX phase, ACS Appl. Nano Mater. 1 (2018) 2455–2460.
[100] R. Meshkian, M. Dahlqvist, J. Lu, B. Wickman, J. Halim, J. Thörnberg, Q. Tao, S. Li, S. Intikhab, J. Snyder, M.W. Barsoum, M. Yildizhan, J. Palisaitis, L. Hultman, P.O.Å. Persson, J. Rosen, W-Based, Atomic laminates and their 2D derivative W1.33C MXene with vacancy ordering, Adv. Mater. 30 (2018), 1706409.
[101] X. Wang, X. Shen, Y. Gao, Z. Wang, R. Yu, L. Chen, Atomic-scale recognition of surface structure and intercalation mechanism of Ti3C2X, J. Am. Chem. Soc. 137 (2015) 2715–2721.
[102] H.-W. Wang, M. Naguib, K. Page, D.J. Wesolowski, Y. Gogotsi, Resolving the structure of Ti3C2Tx MXenes through multilevel structural modeling of the atomic pair distribution function, Chem. Mater. 28 (2016) 349–359.
[103] M.H. Tran, T. Schäfer, A. Shahraei, M. Dürrschnabel, L. Molina-Luna, U.I. Kramm, C.S. Birkel, Adding a new member to the MXene family: synthesis, structure, and electrocatalytic activity for the hydrogen evolution reaction of V4C3Tx, ACS Appl. Energy Mater. 1 (2018) 3908–3914.
[104] B. Anasori, Y. Xie, M. Beidaghi, J. Lu, B.C. Hosler, L. Hultman, P.R.C. Kent, Y. Gogotsi, M.W. Barsoum, Two-dimensional, ordered, double transition metals carbides (MXenes), ACS Nano 9 (2015) 9507–9516.
[105] J. Halim, S. Kota, M.R. Lukatskaya, M. Naguib, M.-Q. Zhao, E.J. Moon, J. Pitock, J. Nanda, S.J. May, Y. Gogotsi, M.W. Barsoum, Synthesis and characterization of 2D molybdenum carbide (MXene), Adv. Funct. Mater. 26 (2016) 3118–3127.
[106] F. Liu, J. Zhou, S. Wang, B. Wang, C. Shen, L. Wang, Q. Hu, Q. Huang, A. Zhou, Preparation of high-purity V2C MXene and electrochemical properties as Li-ion batteries, J. Electrochem. Soc. 164 (2017) A709–A713.
[107] F. Du, H. Tang, L. Pan, T. Zhang, H. Lu, J. Xiong, J. Yang, C. Zhang, Environmental friendly scalable production of colloidal 2D titanium carbonitride MXene with minimized nanosheets restacking for excellent cycle life lithium-ion batteries, Electrochim. Acta 235 (2017) 690–699.
[108] J. Yang, M. Naguib, M. Ghidiu, L.-M. Pan, J. Gu, J. Nanda, J. Halim, Y. Gogotsi, M.W. Barsoum, Two-dimensional Nb-based M4C3 solid solutions (MXenes), J. Am. Ceram. Soc. 99 (2016) 660–666.
[109] H. Wang, L. Shi, T. Yan, J. Zhang, Q. Zhong, D. Zhang, Design of graphene-coated hollow mesoporous carbon spheres as high performance electrodes for capacitive deionization, J. Mater. Chem. A 2 (2014) 4739–4750.
[110] A. Feng, Y. Yu, F. Jiang, Y. Wang, L. Mi, Y. Yu, L. Song, Fabrication and thermal stability of NH4HF2-etched Ti3C2 MXene, Ceram. Int. 43 (2017) 6322–6328.
[111] P. Urbankowski, B. Anasori, T. Makaryan, D. Er, S. Kota, P.L. Walsh, M. Zhao, V.B. Shenoy, M.W. Barsoum, Y. Gogotsi, Synthesis of two-dimensional titanium nitride Ti4N3 (MXene), Nanoscale 8 (2016) 11385–11391.
[112] Y.-C. Zhou, L.-F. He, Z.-J. Lin, J.-Y. Wang, Synthesis and structure–property relationships of a new family of layered carbides in Zr-Al(Si)-C and Hf-Al(Si)-C systems, J. Eur. Ceram. Soc. 33 (2013) 2831–2865.
[113] Y. Wu, P. Nie, J. Wang, H. Dou, X. Zhang, Few-layer MXenes delaminated via high-energy mechanical milling for enhanced sodium-ion batteries performance, ACS Appl. Mater. Interfaces 9 (2017) 39610–39617.
[114] O. Mashtalir, M. Naguib, V.N. Mochalin, Y. Dall'Agnese, M. Heon, M.W. Barsoum, Y. Gogotsi, Intercalation and delamination of layered carbides and carbonitrides, Nat. Commun. 4 (2013) 1716.
[115] T. Zhang, L. Pan, H. Tang, F. Du, Y. Guo, T. Qiu, J. Yang, Synthesis of two-dimensional Ti3C2Tx MXene using HCl+LiF etchant: enhanced exfoliation and delamination, J. Alloys Compd. 695 (2017) 818–826.
[116] R.M. Ronchi, J.T. Arantes, S.F. Santos, Synthesis, structure, properties and applications of MXenes: current status and perspectives, Ceram. Int. 45 (2019) 18167–18188.
[117] P. Srimuk, F. Kaasik, B. Krüner, A. Tolosa, S. Fleischmann, N. Jäckel, M.C. Tekeli, M. Aslan, M.E. Suss, V. Presser, MXene as a novel intercalation-type pseudocapacitive cathode and anode for capacitive deionization, J. Mater. Chem. A 4 (2016) 18265–18271.
[118] P. Srimuk, J. Halim, J. Lee, Q. Tao, J. Rosen, V. Presser, Two-dimensional molybdenum carbide (MXene) with divacancy ordering for brackish and seawater desalination via cation and anion intercalation, ACS Sustain. Chem. Eng. 6 (2018) 3739–3747.
[119] W. Bao, X. Tang, X. Guo, S. Choi, C. Wang, Y. Gogotsi, G. Wang, Porous cryo-dried MXene for efficient capacitive deionization, Joule 2 (2018) 778–787.

[120] B. Chen, A. Feng, R. Deng, K. Liu, Y. Yu, L. Song, MXene as a cation-selective cathode material for asymmetric capacitive deionization, ACS Appl. Mater. Interfaces 12 (2020), 13750.
[121] M. Naguib, R.R. Unocic, B.L. Armstrong, J. Nanda, Large-scale delamination of multi-layers transition metal carbides and carbonitrides "MXenes", Dalton Trans. 44 (2015) 9353–9358.
[122] S. Xiaojie, All-MXene-based integrated membrane electrode constructed using $Ti_3C_2T_x$ as an intercalating agent for high-performance desalination, 4554-4563-2020, Environ. Sci. Technol. 54 (2020), 4554 no.4557.
[123] X. Wang, S. Kajiyama, H. Iinuma, E. Hosono, S. Oro, I. Moriguchi, M. Okubo, A. Yamada, Pseudocapacitance of MXene nanosheets for high-power sodium-ion hybrid capacitors, Nat. Commun. 6 (2015) 6544.
[124] R.B. Rakhi, B. Ahmed, D. Anjum, H.N. Alshareef, Direct chemical synthesis of MnO2 nanowhiskers on transition-metal carbide surfaces for supercapacitor applications, ACS Appl. Mater. Interfaces 8 (2016) 18806–18814.
[125] Q.X. Xia, N.M. Shinde, J.M. Yun, T. Zhang, R.S. Mane, S. Mathur, K.H. Kim, Bismuth Oxychloride/MXene symmetric supercapacitor with high volumetric energy density, Electrochim. Acta 271 (2018) 351–360.
[126] B. Chen, A. Feng, K. Liu, J. Wu, Y. Yu, L. Song, Subsize Ti3C2Tx derived from molten-salt synthesized Ti3AlC2 for enhanced capacitive deionization, Ceram. Int. 47 (2021) 3665–3670.
[127] A. Feng, Y. Yu, Y. Wang, F. Jiang, Y. Yu, L. Mi, L. Song, Two-dimensional MXene Ti3C2 produced by exfoliation of Ti3AlC2, Mater. Des. 114 (2017) 161–166.
[128] X. Sang, Y. Xie, M.-W. Lin, M. Alhabeb, K.L. Van Aken, Y. Gogotsi, P.R.C. Kent, K. Xiao, R.R. Unocic, Atomic defects in monolayer titanium carbide (Ti3C2Tx) MXene, ACS Nano 10 (2016) 9193–9200.
[129] B. Han, G. Cheng, Y.K. Wang, X.K. Wang, Structure and functionality design of novel carbon and faradaic electrode materials for high-performance capacitive deionization, Chem. Eng. J. 360 (2019) 364.
[130] B. Chen, A. Feng, R. Deng, K. Liu, Y. Yu, L. Song, MXene as a cation-selective cathode material for asymmetric capacitive deionization, ACS Appl. Mater. Interfaces 12 (2020) 13750–13758.
[131] B. Chen, A. Feng, K. Liu, J. Wu, Y. Yu, L. Song, High-performance capacitive deionization using 3D porous Ti3C2Tx with improved conductivity, J. Electroanal. Chem. 895 (2021), 115515.
[132] S. Wang, G. Wang, X. Che, S. Wang, C. Li, D. Li, Y. Zhang, Q. Dong, J. Qiu, Enhancing the capacitive deionization performance of NaMnO2 by interface engineering and redox-reaction, Environ. Sci.: Nano 6 (2019) 2379–2388.
[133] M. Torkamanzadeh, L. Wang, Y. Zhang, Ö. Budak, P. Srimuk, V. Presser, MXene/activated-carbon hybrid capacitive deionization for permselective ion removal at low and high salinity, ACS Appl. Mater. Interfaces 12 (2020) 26013–26025.
[134] L. Guo, X. Wang, Z.Y. Leong, R. Mo, L. Sun, H.Y. Yang, Ar plasma modification of 2D MXene Ti3C2Tx nanosheets for efficient capacitive desalination, FlatChem 8 (2018) 17–24.
[135] G. Bharath, A. Hai, K. Rambabu, D. Savariraj, Y. Ibrahim, F. Banat, The fabrication of activated carbon and metal-carbide 2D framework-based asymmetric electrodes for the capacitive deionization of Cr(vi) ions toward industrial wastewater remediation, Environ. Sci. J. Integr. Environ. Res.: Water Res. & Technol. 6 (2020) 351–361.
[136] J. Zhang, W. Guo, Q. Guo, L. Jin, Z. Liu, S. Hu, On-site separation of Cr(vi) and Cr(iii) in natural waters by parallel cartridge ion-exchange columns, RSC Adv. 7 (2017) 50657–50662.
[137] Y.-T. Liu, X.-D. Zhu, L. Pan, Hybrid architectures based on 2D MXenes and low-dimensional inorganic nanostructures: methods, synergies, and energy-related applications, Small 14 (2018), 1803632.
[138] K. Lu, Z. Hu, Z. Xiang, J. Ma, B. Song, J. Zhang, H. Ma, Cation intercalation in manganese oxide nanosheets: effects on lithium and sodium storage, Angew. Chem. 128 (2016) 10604–10608.
[139] S. Hand, R.D. Cusick, Characterizing the impacts of deposition techniques on the performance of MnO2 cathodes for sodium electrosorption in hybrid capacitive deionization, Environ. Sci. Technol. 51 (2017) 12027–12034.
[140] B. Liu, L. Yu, F. Yu, J. Ma, In-situ formation of uniform V2O5 nanocuboid from V2C MXene as electrodes for capacitive deionization with higher structural stability and ion diffusion ability, Desalination 500 (2021), 114897.
[141] W. Luo, Y. Gong, Y. Zhu, Y. Li, Y. Yao, Y. Zhang, K. Fu, G. Pastel, C.-F. Lin, Y. Mo, E.D. Wachsman, L. Hu, Reducing interfacial resistance between garnet-structured solid-state electrolyte and Li-metal anode by a germanium layer, Adv. Mater. 29 (2017), 1606042.
[142] R. Malik, Maxing out water desalination with MXenes, Joule 2 (2018) 591–593.
[143] V. Augustyn, Y. Gogotsi, 2D materials with nanoconfined fluids for electrochemical energy storage, Joule 1 (2017) 443–452.
[144] P. Karthikeyan, S.S. Elanchezhiyan, J. Preethi, K. Talukdar, S. Meenakshi, C.M. Park, Two-dimensional (2D) Ti3C2Tx MXene nanosheets with superior adsorption behavior for phosphate and nitrate ions from the aqueous environment, Ceram. Int. 47 (2021) 732–739.
[145] W. Bao, L. Liu, C. Wang, S. Choi, D. Wang, G. Wang, Facile synthesis of crumpled nitrogen-doped MXene nanosheets as a new sulfur host for lithium–sulfur batteries, Adv. Energy Mater. 8 (2018), 1702485.
[146] Y. Wen, T.E. Rufford, X. Chen, N. Li, M. Lyu, L. Dai, L. Wang, Nitrogen-doped Ti3C2Tx MXene electrodes for high-performance supercapacitors, Nano Energy 38 (2017) 368–376.
[147] Y. Yoon, M. Lee, S.K. Kim, G. Bae, W. Song, S. Myung, J. Lim, S.S. Lee, T. Zyung, K.-S. An, A strategy for synthesis of carbon nitride induced chemically doped 2D MXene for high-performance supercapacitor electrodes, Adv. Energy Mater. 8 (2018), 1703173.
[148] C. Yang, Y. Tang, Y. Tian, Y. Luo, M. Faraz Ud Din, X. Yin, W. Que, Flexible nitrogen-doped 2D titanium carbides (MXene) films constructed by an ex situ solvothermal method with extraordinary volumetric capacitance, Adv. Energy Mater. 8 (2018), 1802087.
[149] A. Amiri, Y. Chen, C. Bee Teng, M. Naraghi, Porous nitrogen-doped MXene-based electrodes for capacitive deionization, Energy Storage Mater. 25 (2020) 731–739.
[150] S. Anwer, D.H. Anjum, S. Luo, Y. Abbas, B. Li, S. Iqbal, K. Liao, 2D Ti3C2Tx MXene nanosheets coated cellulose fibers based 3D nanostructures for efficient water desalination, Chem. Eng. J. 406 (2021), 126827.
[151] Y. Luo, G.-F. Chen, L. Ding, X. Chen, L.-X. Ding, H. Wang, Efficient electrocatalytic N2 fixation with MXene under ambient conditions, Joule 3 (2019) 279–289.
[152] X. Sang, Y. Xie, D.E. Yilmaz, R. Lotfi, M. Alhabeb, A. Ostadhossein, B. Anasori, W. Sun, X. Li, K. Xiao, In situ atomistic insight into the growth mechanisms of single layer 2D transition metal carbides, Nat. Commun. 9 (2018) 1–9.
[153] N.E. Mansoor, L.A. Diaz, C.E. Shuck, Y. Gogotsi, T.E. Lister, D. Estrada, Removal and recovery of ammonia from simulated wastewater using Ti3C2Tx MXene in flow electrode capacitive deionization, npj Clean Water 5 (2022) 26.
[154] Z. Chen, X. Xu, Z. Ding, K. Wang, X. Sun, T. Lu, M. Konarova, M. Eguchi, J.G. Shapter, L. Pan, Y. Yamauchi, Ti3C2 MXenes-derived NaTi2(PO4)3/MXene nanohybrid for fast and efficient hybrid capacitive deionization performance, Chem. Eng. J. 407 (2021), 127148.
[155] S. Zhang, X. Xu, X. Liu, Q. Yang, N. Shang, X. Zhao, X. Zang, C. Wang, Z. Wang, J.G. Shapter, Y. Yamauchi, Heterointerface Optimization in a Covalent Organic Framework-On-MXene for High-Performance Capacitive Deionization of Oxygenated Saline Water, Materials Horizons, 2022.
[156] L. Agartan, K. Hantanasirisakul, S. Buczek, B. Akuzum, K.A. Mahmoud, B. Anasori, Y. Gogotsi, E.C. Kumbur, Influence of operating conditions on the desalination performance of a symmetric pre-conditioned Ti3C2Tx-MXene membrane capacitive deionization system, Desalination 477 (2020), 114267.
[157] J. Ai, J. Li, K. Li, F. Yu, J. Ma, Highly flexible, self-healable and conductive poly(vinyl alcohol)/Ti3C2Tx MXene film and it's application in capacitive deionization, Chem. Eng. J. 408 (2021), 127256.
[158] M. Liang, L. Wang, V. Presser, X. Dai, F. Yu, J. Ma, Combining battery-type and pseudocapacitive charge storage in Ag/Ti3C2Tx MXene electrode for capturing chloride ions with high capacitance and fast ion transport, Adv. Sci. 7 (2020), 2000621.
[159] J. Ma, Y. Cheng, L. Wang, X. Dai, F. Yu, Free-standing Ti3C2Tx MXene film as binder-free electrode in capacitive deionization with an ultrahigh desalination capacity, Chem. Eng. J. 384 (2020), 123329.
[160] S. Buczek, M.L. Barsoum, S. Uzun, N. Kurra, R. Andris, E. Pomerantseva, K.A. Mahmoud, Y. Gogotsi, Rational design of titanium carbide MXene electrode architectures for hybrid capacitive deionization, Energy & Environ. Mater. 3 (2020) 398–404.

[161] K.B. Hatzell, M.C. Hatzell, K.M. Cook, M. Boota, G.M. Housel, A. McBride, E.C. Kumbur, Y. Gogotsi, Effect of oxidation of carbon material on suspension electrodes for flow electrode capacitive deionization, Environ. Sci. Technol. 49 (2015) 3040–3047.
[162] P. Długołęcki, A. van der Wal, Energy recovery in membrane capacitive deionization, Environ. Sci. Technol. 47 (2013) 4904–4910.
[163] Y. Cai, X. Cao, Z. Luo, G. Fang, F. Liu, J. Zhou, A. Pan, S. Liang, Caging Na3V2(PO4)2F3 microcubes in cross-linked graphene enabling ultrafast sodium storage and long-term cycling, Adv. Sci. 5 (2018), 1800680.
[164] M. Pasta, C.D. Wessells, Y. Cui, F. La Mantia, A desalination battery, Nano Lett. 12 (2012) 839–843.
[165] H. Yoon, J. Lee, S. Kim, J. Yoon, Hybrid capacitive deionization with Ag coated carbon composite electrode, Desalination 422 (2017) 42–48.
[166] A. VahidMohammadi, M. Mojtabavi, N.M. Caffrey, M. Wanunu, M. Beidaghi, 2D MXenes: assembling 2D MXenes into highly stable pseudocapacitive electrodes with high power and energy densities (adv. Mater. 8/2019), Adv. Mater. 31 (2019), 1970057.
[167] K. Zhu, H. Zhang, K. Ye, W. Zhao, J. Yan, K. Cheng, G. Wang, B. Yang, D. Cao, Two-dimensional titanium carbide MXene as a capacitor-type electrode for rechargeable aqueous Li-ion and Na-ion capacitor batteries, Chemelectrochem 4 (2017) 3018–3025.
[168] M.R. Lukatskaya, O. Mashtalir, C.E. Ren, Y. Dall'Agnese, P. Rozier, P.L. Taberna, M. Naguib, P. Simon, M.W. Barsoum, Y. Gogotsi, Cation intercalation and high volumetric capacitance of two-dimensional titanium carbide, Science 341 (2013) 1502–1505.
[169] J. Come, J.M. Black, M.R. Lukatskaya, M. Naguib, M. Beidaghi, A.J. Rondinone, S.V. Kalinin, D.J. Wesolowski, Y. Gogotsi, N. Balke, Controlling the actuation properties of MXene paper electrodes upon cation intercalation, Nano Energy 17 (2015) 27–35.
[170] J.N. Coleman, M. Lotya, A. O'Neill, S.D. Bergin, P.J. King, U. Khan, K. Young, A. Gaucher, S. De, R.J. Smith, I.V. Shvets, S.K. Arora, G. Stanton, H.-Y. Kim, K. Lee, G.T. Kim, G.S. Duesberg, T. Hallam, J.J. Boland, J.J. Wang, J.F. Donegan, J.C. Grunlan, G. Moriarty, A. Shmeliov, R.J. Nicholls, J.M. Perkins, E. M. Grieveson, K. Theuwissen, D.W. McComb, P.D. Nellist, V. Nicolosi, Two-dimensional nanosheets produced by liquid exfoliation of layered materials, Science 331 (2011) 568–571.
[171] Y. Xie, P.R.C. Kent, Hybrid density functional study of structural and electronic properties of functionalized Ti${ }_{n+1}{X}_{n}$ ($X=\mathrm{C}$, N) monolayers, Phys. Rev. B 87 (2013), 235441.
[172] A. Feng, Y. Yu, L. Mi, Y. Yu, L. Song, Comparative study on electrosorptive behavior of NH4HF2-etched Ti3C2 and HF-etched Ti3C2 for capacitive deionization, Ionics 25 (2019) 727–735.
[173] M.A. Hope, A.C. Forse, K.J. Griffith, M.R. Lukatskaya, M. Ghidiu, Y. Gogotsi, C.P. Grey, NMR reveals the surface functionalisation of Ti3C2 MXene, Phys. Chem. Chem. Phys. 18 (2016) 5099–5102.
[174] M. Qin, A. Deshmukh, R. Epsztein, S.K. Patel, O.M. Owoseni, W.S. Walker, M. Elimelech, Comparison of energy consumption in desalination by capacitive deionization and reverse osmosis, Desalination 455 (2019) 100–114.
[175] A. Al-Karaghouli, L.L.J.R. Kazmerski, S.E. Reviews, Energy consumption and water production cost of conventional and, Renew. -Energy-Powered Desalination Processes 24 (2013) 343–356.
[176] P.G. Youssef, R.K. Al-Dadah, S.M. Mahmoud, Comparative analysis of desalination technologies, Energy Proc. 61 (2014) 2604–2607.
[177] J. Elisadiki, T.E. Kibona, R.L. Machunda, M.W. Saleem, W.-S. Kim, Y.A.C. Jande, Biomass-based carbon electrode materials for capacitive deionization: a review, Biomass Conversion and Biorefinery 10 (2020) 1327–1356.
[178] D.M. Warsinger, J. Swaminathan, E. Guillen-Burrieza, H.A.J.D. Arafat, in: Scaling and Fouling in Membrane Distillation for Desalination Applications: a Review, vol. 356, 2015, pp. 294–313.
[179] S. Porada, L. Borchardt, M. Oschatz, M. Bryjak, J.S. Atchison, K.J. Keesman, S. Kaskel, P.M. Biesheuvel, V. Presser, Direct prediction of the desalination performance of porous carbon electrodes for capacitive deionization, Energy Environ. Sci. 6 (2013) 3700–3712.
[180] I. Cohen, E. Avraham, Y. Bouhadana, A. Soffer, D. Aurbach, Long term stability of capacitive de-ionization processes for water desalination: the challenge of positive electrodes corrosion, Electrochim. Acta 106 (2013) 91–100.
[181] A. Omosebi, X. Gao, J. Landon, K.L. Liu, Asymmetric electrode configuration for enhanced membrane capacitive deionization, ACS Appl. Mater. Interfaces 6 (2014), 12640.
[182] N. Holubowitch, A. Omosebi, X. Gao, J. Landon, K. Liu, Quasi-steady-state polarization reveals the interplay of capacitive and faradaic processes in capacitive deionization, Chemelectrochem 4 (2017) 2404–2413.
[183] X. Gao, A. Omosebi, J. Landon, K. Liu, Surface charge enhanced carbon electrodes for stable and efficient capacitive deionization using inverted adsorption–desorption behavior, Energy Environ. Sci. 8 (2015) 897–909.
[184] K.B. Hatzell, E. Iwama, A. Ferris, B. Daffos, K. Urita, T. Tzedakis, F. Chauvet, P.-L. Taberna, Y. Gogotsi, P. Simon, Capacitive deionization concept based on suspension electrodes without ion exchange membranes, Electrochem. Commun. 43 (2014) 18–21.
[185] W. Bao, X. Tang, X. Guo, S. Choi, C. Wang, Y. Gogotsi, G. Wang, Porous cryo-dried MXene for efficient capacitive deionization, Joule 2 (2018) 778.
[186] A. Lipatov, M. Alhabeb, M.R. Lukatskaya, A. Boson, Y. Gogotsi, A. Sinitskii, Effect of synthesis on quality, electronic properties and environmental stability of individual monolayer Ti3C2 MXene flakes, Adv. Electron. Mater. 2 (2016), 1600255.
[187] C.E. Shuck, M. Han, K. Maleski, K. Hantanasirisakul, S.J. Kim, J. Choi, W.E.B. Reil, Y. Gogotsi, Effect of Ti3AlC2 MAX phase on structure and properties of resultant Ti3C2Tx MXene, ACS Appl. Nano Mater. 2 (2019) 3368–3376.
[188] C.J. Zhang, S. Pinilla, N. McEvoy, C.P. Cullen, B. Anasori, E. Long, S.-H. Park, A. Seral-Ascaso, A. Shmeliov, D. Krishnan, C. Morant, X. Liu, G.S. Duesberg, Y. Gogotsi, V. Nicolosi, Oxidation stability of colloidal two-dimensional titanium carbides (MXenes), Chem. Mater. 29 (2017) 4848–4856.
[189] T. Habib, X. Zhao, S.A. Shah, Y. Chen, W. Sun, H. An, J.L. Lutkenhaus, M. Radovic, M.J. Green, Oxidation stability of Ti3C2Tx MXene nanosheets in solvents and composite films, npj 2D Mater. Appl. 3 (2019) 8.